Diploma Thesis

In vivo Investigation of Gemcitabine-IPs:
Effects on the rate of C6-Glioblastoma rat cell proliferation in the Chicken Chorioallantoic Membrane Model

submitted by

Sandro Stojanović

for the acquisition of the Academic Degree

Doctor of Medicine

(Dr. med. univ.)

at the

Medical University of Graz

conducted at the

Department of Neurosurgery

Research Unit Experimental Neurotraumatology

under the supervision of

Sen. Scientist Priv.-Doz. Dr. rer. nat. Silke Patz

Linda Waldherr, MSc. PhD.

Graz, 20th of November 2021

Statutory Declaration

I declare that I have authored this thesis independently, that I have not used other than the declared sources/resources, and that I have explicitly marked all material which has been quoted either literally or by content from the used sources.

Graz, 20th of November 2021 Sandro Stojanović eh.

Preface

This diploma thesis has been written and submitted in partial fulfilment of the requirements for the degree of Dr. med. univ. at the Medical University of Graz. I was engaged in the research project from September 2020 to June 2021 and worked on my thesis during this period.

Having grown up with frequent visits to doctor's offices and hospitals during my childhood, the hospital has not always been the place I would consider as my favorite one. And even less as my future working place. To be honest, during my childhood visiting hospitals or doctors became the most horrifying situation I could imagine to be in.

My desire to become a doctor was born around the age of fifteen after a close relative had been diagnosed with a brain tumor and passed away shortly after the diagnosis. An operation could not bring any improvements and the relative's condition worsened rapidly. He began losing his memory and was not even able to recognize faces anymore at all – neither his wife's nor his children's. Although there was one name the tumor had not been able to make him forget – it was mine.

Not only have I experienced the cruelty of cancer that day, but rather realized how incredible the human mind can be. In particular, an emerging interest for the complexity of the human brain was born. In the years thereafter, I repeatedly came in touch with brain tumors – whether it was within close acquaintances' families or during clinical traineeships. Despite the frequency and malignancy, treatment options and prognosis barely enhanced over time.

All of that is where my motivation for this project and thesis originally stemmed from – to see, learn and understand what makes this cancer unique; to see what the future has prepared to eventually overcome the hurdle called „brain cancer.

Acknowledgement

First and foremost, I would like to express my deep and sincere gratitude to my research supervisor Sen. Scientist Priv.-Doz. Dr. rer. nat. Silke Patz, Laboratory Head of the Research Unit for Experimental Neurotraumatology, for giving me the opportunity to be part of this innovative project and providing invaluable guidance throughout this research.

Another very special thanks goes to MSc Handl Verena who allowed me to accompany her in every task and spared no effort to teach and support me in all respects; whether it was in practical matters or theoretical know-how.
I am extending my heartfelt thanks to Dr. rer. nat. Nassim Ghaffari, MSc PhD. Linda Waldherr and Mrs. Waltraud Huber – for their warm and hospitable reception into the team as well as their incredible collegiality and helpfulness in a to me totally new field of work. It was an honor and great privilege to work with all of you!

Subsequently, I am extremely grateful to everyone who ever played a role in my academic accomplishments. Thanks to my sister and parents for their love and sacrifices to educate and prepare me for my future. Thanks to my family and friends for their endless support and strong faith in me.

Table of Contents

List of abbreviations

ABBREVIATIONS	MEANING
CAM	Chorioallantoic membrane
CNS	Central nervous system
GBM	Glioblastoma Multiforme
GEMIP	Gemcitabine iontronic pump
HE, H&E	Hematoxylin and eosin
IEM	Ion exchange membrane
IFRT	Involved field radiation therapy
IP	Iontronic pump
OIEP	Organic electronic ion pumps
OS	Overall survival
PBS	Phosphate buffered saline
PFA	Paraformaldehyde
TMZ	Temozolomide
VEGFR-2	Vascular endothelial growth factor receptor 2
WHO	World health organization

List of figures

List of tables

Zusammenfassung

Das Glioblastoma Multiforme (GBM) ist der am häufigsten auftretende und gleichzeitig bösartigste Tumor im Bereich des Gehirns. Sein schnelles sowie infiltratives Wachstum, die Schwierigkeit der vollständigen Tumorentfernung und der Mangel an effektiven therapeutischen Alternativen machen ihn zu einem der tödlichsten Tumorerkrankung überhaupt. Die gegenwärtige Therapie des GBM setzt sich zusammen aus einer maximal möglichen Tumorresektion kombiniert mit adjuvanter Involved-Field-Radiatio und Temozolomid-Chemotherapie. Trotz des multimodalen Behandlungskonzepts gab es in den letzten Jahrzehnten keine signifikante Verbesserung der Prognose oder mittleren Überlebensrate.

Ein vielversprechender Ansatz für neue Behandlungsmöglichkeiten wäre eine lokale Behandlung mittels eigens entwickelter Ionenpumpe. Diese würde postoperativ ins Resektionsareal eingesetzt werden und über ein induzierbares elektromagnetisches Feld eine direkte Medikamentenapplikation im Zielgewebe ermöglichen.

Bevor so ein Konzept am Menschen realisiert werden kann, sind zunächst einige Zwischenschritte erforderlich. Die durchgeführte Versuchsreihe hat deshalb zum Zweck, den Effekt einer Gemzitabin-Ionenpumpe auf Ratten-Glioblastoma-C6-Zellen im Chorioallantoic Membrane (CAM) Modell zu überprüfen.
Das CAM-Assay bietet ein kostengünstiges und schnell reproduzierbares in-vivo Modell für die Tumorforschung. Die C6-Ratten-Zellen werden aufgrund verschiedenster Vorteile als Goldstandard in der GBM-Forschung herangezogen.

Die C6-Zellen wurden mittels Silikonring auf die CAM transplantiert, unterschiedlichen Behandlungen ausgesetzt und die gezüchteten Tumore schließlich wieder herausgeschnitten. Es folgte eine histologische sowie immunhistochemische Analyse.

Um die Effektivität der Gemzitabin-Ionenpumpe darzulegen, wurde der Ki-67 Proliferationsindex der unterschiedlich behandelten Tumore bestimmt und statistisch ausgewertet.

Abstract

The Glioblastoma Multiforme (GBM) is the most frequently occurring and simultaneously most malignant tumor of the brain. His rapid and highly invasive growth behaviour, the difficulty of complete tumor removal and the lack of effective therapeutical options make him one of the deadliest neoplasms in general. The current therapy for GBM consists of maximal safe tumor resection followed by adjuvant involved field radiation and chemotherapy with temozolomide. Despite a multimodal treatment approach, the overall survival and prognosis did not show significant improvement in recent decades.

A very promising attempt to improve therapy success is a drug delivery device for local treatment. The specially developed iontronic pump could be implanted into the surgical cavity postoperatively and deliver substances directly to the targeted area by induction of an electromagnetic field.

To establish such a concept for human patients, many intermediate steps are required before. The aim of the accomplished experimental series is to investigate the effects of a gemcitabine iontronic pump on C6 rat glioblastoma cells in the chicken chorioallantoic membrane (CAM) model.
The CAM assay provides a cost-effective and easily reproducible in-vivo model for cancer research. The C6 rat cells remain the gold standard in glioma research due to several advantages.

The C6 cells were xenografted on the CAM by the help of silicon rings, received different treatment conditions and subsequently the cultured tumors were harvested. A histological and immunohistochemical analysis followed.

To examine the effects of the gemcitabine iontronic pump, the Ki-67 proliferation index of the different treated tumors was determined and statistically evaluated.

1. INTRODUCTION

1.1 Glioma

The term glioma defines neoplasms originating from so-called glial cells of the brain or spine. As the most frequent neoplasm of the CNS and especially in the brain, the incidence ranges from 5 to 10 per 100.000 people – affecting all age-groups, especially the elderly with a peak in the 6th-7th life decade [1].

The further classification of gliomas depends on their tumor grade, cell origin and location. Regarding the tumor grade, gliomas can be either well-differentiated (low-grade, non-anaplastic) or undifferentiated (high-grade, anaplastic). Regarding the location, gliomas can grow supratentorial (above the tentorium) or infratentorial (below the tentorium). Regarding the cell origin, glia cells can be categorized in different cell types as ependymal cells (ependymoma), astrocytes (astrocytoma) or oligodendrocytes (oligodendroglioma) [1].

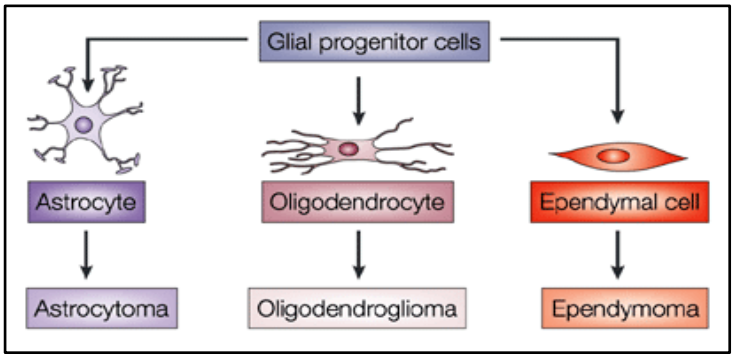

Figure 1: Different types of glia cells [2].

Grade / Type	WHO grade I	WHO grade II	WHO grade III	WHO grade IV
	Circumscript	Low-grade	Diffuse / High-grade	
Astrocytoma	Pilocytic astrocytoma	Low-grade astrocytoma	Anaplastic astrocytoma	Glioblastoma
Oligodendroglioma		Low-grade oligodendro-glioma	Anaplastic oligodendro-glioma	
Oligo-astrocytoma		Low-grade oligo-astrocytoma	Anaplastic oligo-astrocytoma	

Figure 2: Classification of gliomas in types and WHO grades [3].

1.2 Glioblastoma Multiforme

With more than 60% of cases the WHO grade IV GBM is the most malignant and most frequent of all primary brain neoplasms. Characteristics are a rapid and infiltrating growth with a fast progression to death – mostly within only 12-18 months from the day of diagnosis. GBM not only has a low sensitivity to radio- and chemotherapy, but also shows – despite immediate and optimal treatment – reoccurrence in all cases. Even though GBM hardly ever shows metastases outside the brain, their invading-pattern by the way of single cells makes surgical intervention barely curative [1]. Histological characteristics are nuclear atypia, high mitotic activity, intense microvascular proliferation and necrosis [4].
Concerning these facts, it is clearly obvious that the GBM is one of the deadliest neoplasms of our time and therefore innovative advances in neurosurgical techniques and novel therapeutic possibilities are required.

1.3 Current Therapies

To approach the complex and heterogenic appearance of GBM, a multimodal concept with several therapeutic strategies as surgical resection, chemoradiation and biological- as well as immunotherapy is used.
The first step in newly diagnosed GBM is a maximal safe surgical resection with the intention to decrease in tumor mass and thus alleviate patient's symptoms caused by the space claim of the growing mass; but also, to acquire tissue for histological and molecular examination. As a greater extent in tumor mass removal is accompanied by an enhancement of survival, a maximal safe resection should be considered in all patients eligible to receive this form of surgery. An adjuvant chemoradiation therapy should follow the chirurgical intervention, consisting of: Involved field radiation therapy (IFRT) and concurrent as well as adjuvant chemotherapy with temozolomide (TMZ). The combination of radiation and chemotherapy shows significant benefits in overall survival (OS) compared to radiation alone [5].

1.3.1 Involved field radiation therapy

The IFRT is aiming directly at the clinical target volume (gross tumor volume + a 2-3cm margin for subclinical microscopic malignant lesions) to maximize treatment to the tumor and decrease damage to surrounding healthy tissue [4]. A total dose of 60 Grey during therapy is not to exceed – fractioned in 2 Gy per day for 5 days a week. There is no evidence for benefits by using total doses over 60 Gy [5].

1.3.2 Temozolomide

Despite the fact that around 50% of patients do not show the desired treatment effect, TMZ remains the most widely used chemotherapy – probably due to the lack of superior treatment options [6]. The TMZ treatment includes 75 mg/m² body surface for six weeks daily prior to another six cycles (one cycle = 28 days) of 150-200 mg/m² body surface for 5 days/cycle. Alternative approaches as brachytherapy, radioactive isotopes (I-125) or stereotactic radiosurgery did not show any significant advantages for overall survival [5].

1.3.3 Gemcitabine in the treatment of GBM

Gemcitabine is a nucleoside analog used as a chemotherapeutic, which operates strongly antitumoral in high-grade glioma (C6) in from of a radiosensitizer [7]. Furthermore, gemcitabine works as inhibitor of DNA chain elongation and enhancer of antitumoral immune activity; but not to neglect disadvantages like short half-time or side effects [8]. It’s currently authorized in the treatment of multiple solid tumors like e.g., ovarian- or pancreatic cancer [9].

However, facing such high mortality and low OS despite multimodal therapy concepts accentuates the importance of developing new anti-tumor strategies for GBM even more. One promising opportunity for a new anti-tumor treatment could be an Ion Pump for selective drug delivery; but, as always before clinical trials for new treatment concepts are practicable, extensive research is inevitable. And with that said, the need of an appropriate in vivo model comes hand in hand: the chicken chorioallantoic membrane model.

1.4 Chicken chorioallantoic membrane (CAM) model

The CAM shows a wide range of benefits for in vivo investigations: comparably simple, cost-effective and especially expeditious with the possibility to screen several specimens simultaneously [10]. What makes this extraembryonic membrane unique is the high vascularization and multiple other functions as gas exchange. Moreover, features like visibility, accessibility and extremely quick development make it attractive for manipulation and therefore for research [11]. However, a nonspecific inflammatory reaction displays the main limitation – mostly in experiments lasting more than 15 days after incubation; but grafting the test-material at a time the host's immune system is still immature (once the CAM starts to develop) can reduce the risk of nonspecific inflammation [10]. Especially in terms of cancer research the CAM provides a microenvironment with blood vessels and stromal tissue as well as distinguishing invasion and angiogenesis [12].

A model for GBM on the CAM showed formation of avascular tumors (within 2 days) prior to rapid progression in form of VEGFR-2-dependent angiogenesis accompanied by necrosis, hemorrhage and peritumoral edema. Moreover, the model displayed clearly perceivable cell invasion as well as the migration of tumor cells along blood vessels. This enables additional advantages for GBM research to other models; like for e.g., observation of real time-changes in tumor morphology by microscopy, as good as non-notable cancer cell damage and thus glioma cell survival until extravasation [13].

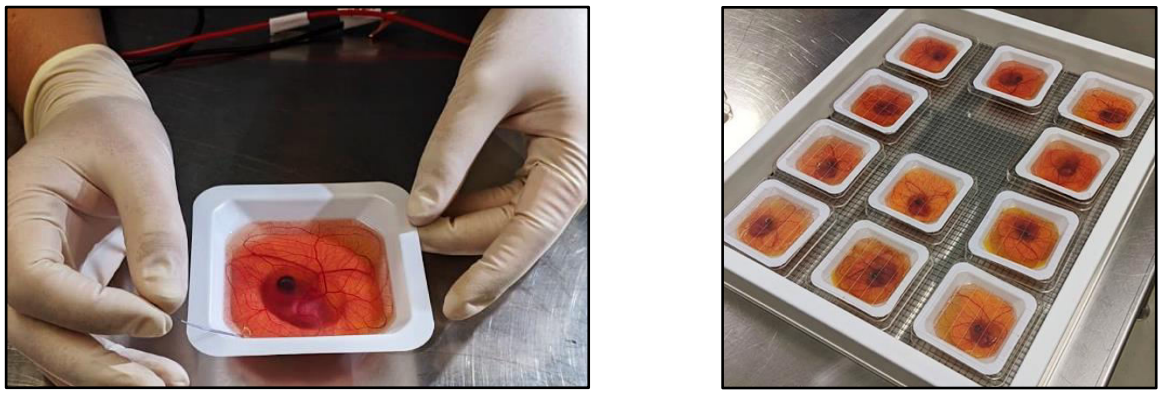

Figure 3: Chicken chorioallantoic membrane (CAM) of an embryo ex ovo

Figure 4: Simultaneous cultivation of several embryos

An ethical approval is not necessary (EU) as the CAM assay is not proclaimed as animal experiment by law and also conforms the 3R criteria – replacement, reduction and refinement [12].

1.5 Drug delivery devices

Drug delivery devices are based on the principle of applying an electromagnetic field over an ion exchange membrane (IEM) in order to build up a driving force for electrophoresis. Starting from an internal drug reservoir, the electrical charged drug goes through the IEM by electrophoresis and enters the addressed treatment area [14]. Especially for the treatment of neurological diseases implantable devices provide an alternative to systemic therapy – an animal model illustrated the suitability even for in vivo cortical delivery by local manipulation of ion concentration [15]. Moreover, the blood-brain barrier can be bypassed as the drug delivery device gets implanted directly in the targeted treatment area [14]. Figure 5 below displays the conditions and the aim of a drug delivered device in a very simple manner; the shown electrodes („+“ and „-“) induce the required electromagnetic field.

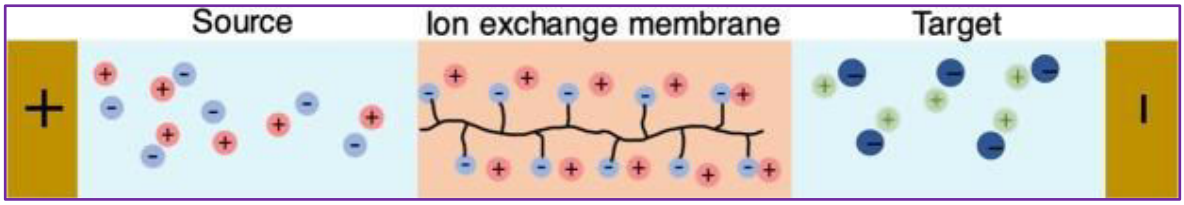

Figure 5: A simplified illustration of the drug delivery device components: Electrodes, source with drug reservoir, IEM and the targeted treatment area [14].

1.5.1 Iontronic Pumps (IPs)/Organic Electronic Ion Pumps (OEIPs)

OEIPs are based on the principles of drug delivery devices; they pump charged particles (drugs) through anion- or cation exchange membranes (IEM) into a targeted area. Remarkably incidental occur features as high spatiotemporal

delivery resolution and tremendous dosage precision ideally without the accompaniment of even minimal liquid transport [16]. For an overview, Figure 6 displays the structure of OIEPs – similar to the iontronic delivery device in Figure 5 – in general terms.

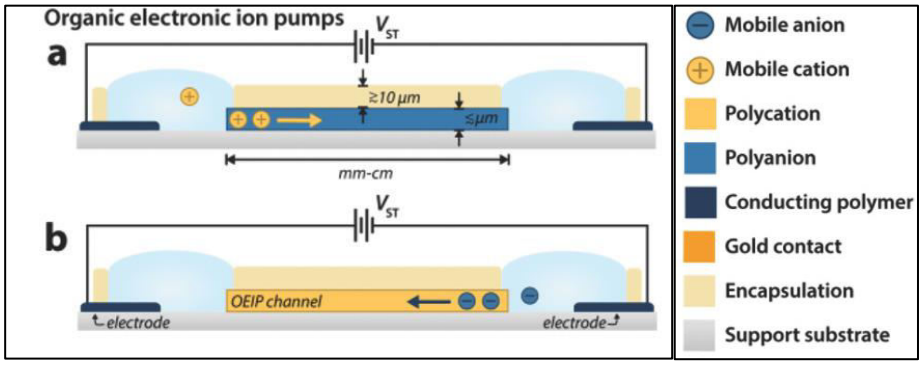

Figure 6: Structure of an IP/OEIP based on the principles of iontronic delivery devices (Figure 5). a) OIEP with selective cation („+“) transport; b) OIEP with selective anion („-“) transport [17].

In this matter, the required IEM is formed by the OEIP channel, which separates the drug reservoir and the addressed treatment area. The ionic current in-/decreases proportionally to alterations of the induced electromagnetic field, whilst resistance and electric resistivity are affected by the geometry of the OEIP channel [17].

1.5.2 Outlook and motives

New OIEPs based on capillary fibers (hyperbranched polyglycerols) as IEM are supposed to make them suitable for a variety of ionic compounds and provide precise tailoring of the channels' fixed charge concentration in the future [18]. Not only should future implants open new possibilities of therapy and treatment for suffering patients, but as well be able to run up to several years [17].

Since the beginning emergence of the drug delivery device and thus the OEIP technology, in 2019 [19] for the first-time efficient delivery of large molecules was managed (in plants). This points out the rapid progress of OEIPs and their wide range of possible usage in the future.

2. Objectives and expectations of the research project

As previously mentioned, the GBM remains one of the deadliest tumors characterized by his massive neoangiogenesis, the rapid progression and a diffuse invading-pattern throughout the brain. The gold standard for treatment and other modern therapy options still do not bring the desired results not only because of the aggressive tumor behavior; but also due to drug resistance, treatment intolerance and inadequate availability of drug concentration at the targeted area.

The ultimate aim of this project is to invent an OEIP, which can be implanted straight into the surgical cavity immediately after resection of the macroscopic visible mass. Then, by the principles of the above explained iontronic delivery device, an applied electromagnetic field should induce the positively charged chemotherapeutic gemcitabine to be „pumped“ into the surgical area – for remaining single cells of the GBM to become extinguished by gemcitabine.

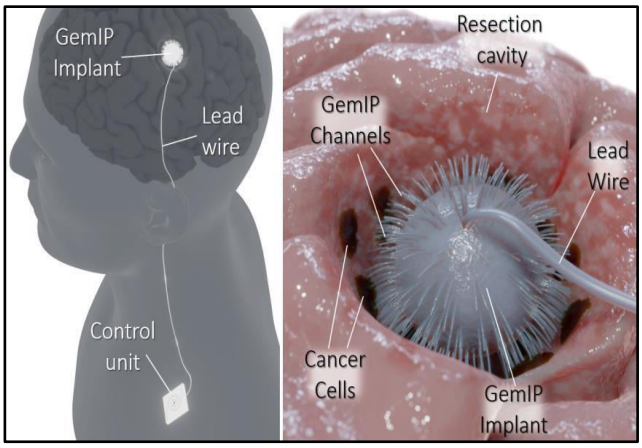

Figure 7: A first draft of a GemIP implant. (kindly provided by Dr. Patz Silke)

We expect – or rather hope – that this new therapeutic approach will finally contribute to decrease the recurrence rate as well as improve the poor prognosis, life quality and OS. And maybe one day even bring a cure for GBM.

However, the previous described the final steps of the project and therefore this anticipation goes a bit too far ahead into the future – as the project is still

somewhere near the beginning. For now, our goal was to prove the functionality of gemcitabine IPs (GemIPs) and their effect on the proliferation rate of glioblastoma cells. To imitate the conditions of tumor growth as accurate as possible, we seeded the cells on the surface of the highly vascularized CAM and in further steps inserted the GemIP.

3. Methods and material

The following section will deal with the implementation of the CAM assay, the histological reprocessing and the immunohistochemical staining – transitioning to the analysis and findings of this study.

3.1 GBM cell line

In general, different glioblastoma cell lines were used for the research in the CAM assay – counting C6, U-251 MG and U-87 MG cell lines for example. U-251 MG and U-87 MG are both human glioblastoma cell lines, whereas C6 is a rat glioblastoma cell line.

The distinction of various glioblastoma cell lines is due to the fact that they present different mutations and specific protein expression-behavior in each case [20]. The human cell lines alone already differ between 48 sustainable subtypes [21]! Nevertheless, the gold standard in glioma research remains the C6 rat cell line as it imitates the character of human glioblastoma comparatively good and does not require immunocompromised models to be developed [22]. This thesis will solely discuss the findings in terms of the C6 glioblastoma rat cell line – to be precise, C6 single cells with a cell count of 10^6 were used.

Table 1: Add-on – GBM cell lines

Cell line:	*C6*	*U-251*	*U-87*
Organism	Rattus norv. (rat)	Homo sap. (human)	Homo sap. (human)
Tissue	Brain	Brain	Brain

Morphology	Fibroblast	Epithelial	Epithelial
Cell type	Glioma	Glioblastoma	Glioblastoma
Growth property	Monolayer, adherent	Monolayer, adherent	Monolayer, adherent

3.2 Chicken Chorioallantoic Membrane Assay

The workflow of an ex ovo CAM assay has to follow a specific timetable – in cooperation with Dr. Ghaffari Nassim the CAM assay was performed at the Institute of Pathophysiology (Graz, Austria) according to her procedure, but in a slightly modified way as we had to insert GemIPs as well. For the purpose of basic understanding, the following Figure depicts the general procedure before going into detail.

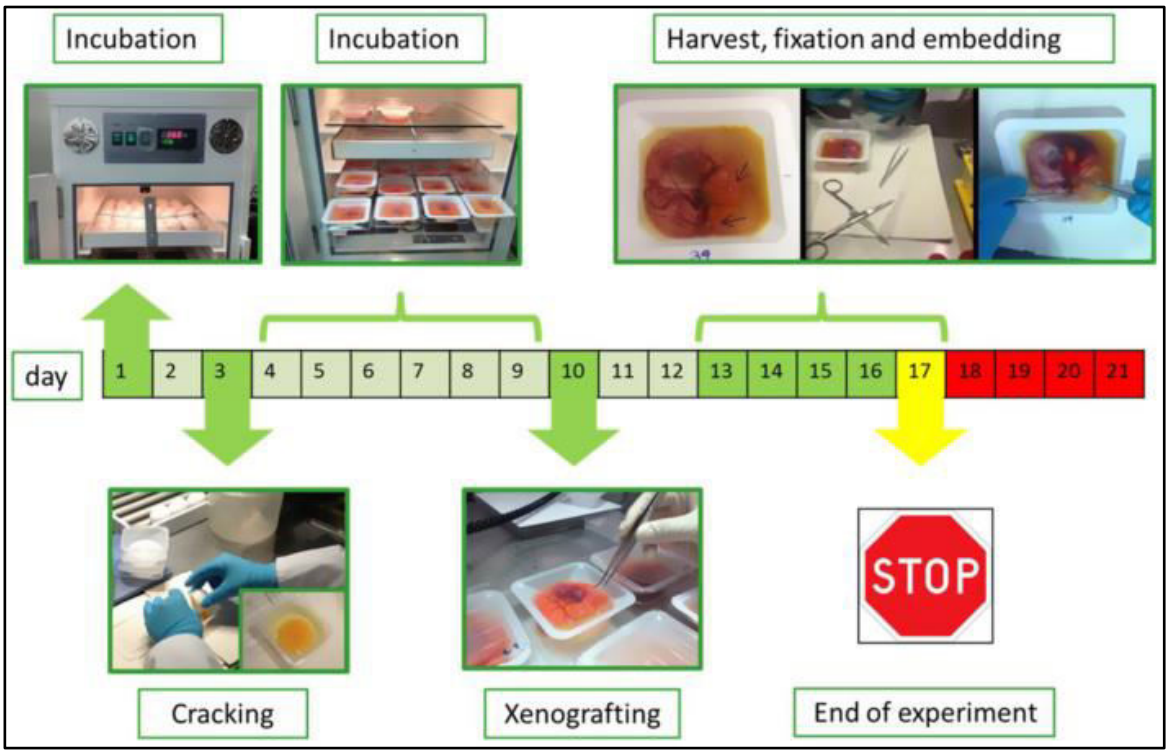

Figure 8: Ex ovo CAM assay – schematic timetable [12].

3.2.1 Preparation of the CAM-Experiment

The day on which the fertilized eggs were delivered determines the starting point of the CAM assay and is therefore marked as day one. By arrival in the laboratory the eggs were washed with warm water and disinfected using an even brush before being incubated – the adjusted incubator had a temperature of 37.6°C and a humidity of about 40-60%.

After two days of incubation the eggshell was cracked and the up till now sealed content carefully shifted into a sterilized plastic petri dish; a germ-/dirt protecting cover was put on top to replace the removed shelter providing eggshell. Since the incubation nudges the egg yolk to gather in the superior section of the egg, it‘s important not to change the egg’s position for the process of cracking – the first impulse then is made by an electrical blade in form of creating a favorable breaking point.

Subsequently, the egg containing petri dishes were put in the incubator for seven more days following the same adjustments as previously mentioned.

3.2.2 Implementation of the CAM-Experiment

On day ten (count-start always in reference to the first egg incubation) the GBM cell line was applied within close proximity to a vascular strand of the CAM and once again incubated before GemIP implantation as well as treatment administration and eventual „tumor” harvesting for analysis followed.

3.2.2.1 Onplants and Xenografting

Autoclaved silicon rings were used for the xenograft of the C6 cells to guarantee a compact growth on the one hand and to facilitate the ensuing onplant harvest on the other hand. First of all, the silicon rings alone were implanted near a vascular branch by the help of tweezers. Then, the C6 cells were applied into each ring by pipetting 10µl of the Geltrex®-cell-mix with a precooled pipette; before the xenografted embryos were incubated once again (37.6°C, 40-60% humidity).

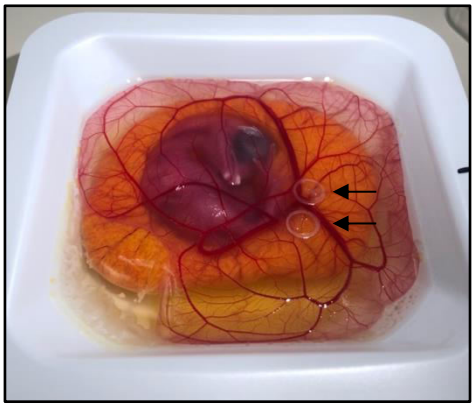

a) overview

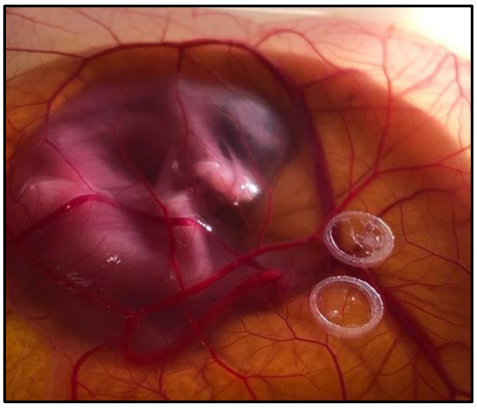

b) close up

3.2.2.2 GemIPs and Treatment

Figure 9: Xenografted silicon rings – a) black arrows point to two transplanted onplants on an CAM; b) close-up of the rings displaying the tumor growth inside (day 14).

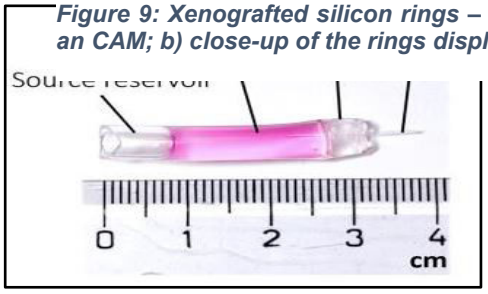

Figure 10: GemIP – a schematic design (kindly provided by Dr. Patz Silke!)

icon

wed

and photographed under the microscope to determine their growth behavior previous to further application. One fraction of subjects got a GemIP + an extra electrode – to induce the electromagnetic field – implanted through the upper cover; an illustration of an embryo treated with a GemIP is shown in Fig. 11. Another fraction remained untreated, whilst the rest received different treatment conditions at different times: One group was irradiated (72h OR 30min prior to harvesting); a second was treated manually with Gemcitabine by pipetting the substance (1d after seeding OR 4h prior to harvesting); the next got a concurrent therapy consisting of radiation and Gemcitabine manually; as positive control, the remaining embryos were treated with Cytidine manually OR in form of a CytIP 1d after seeding. Regarding treatment and time, we had a total of 10 conditions.

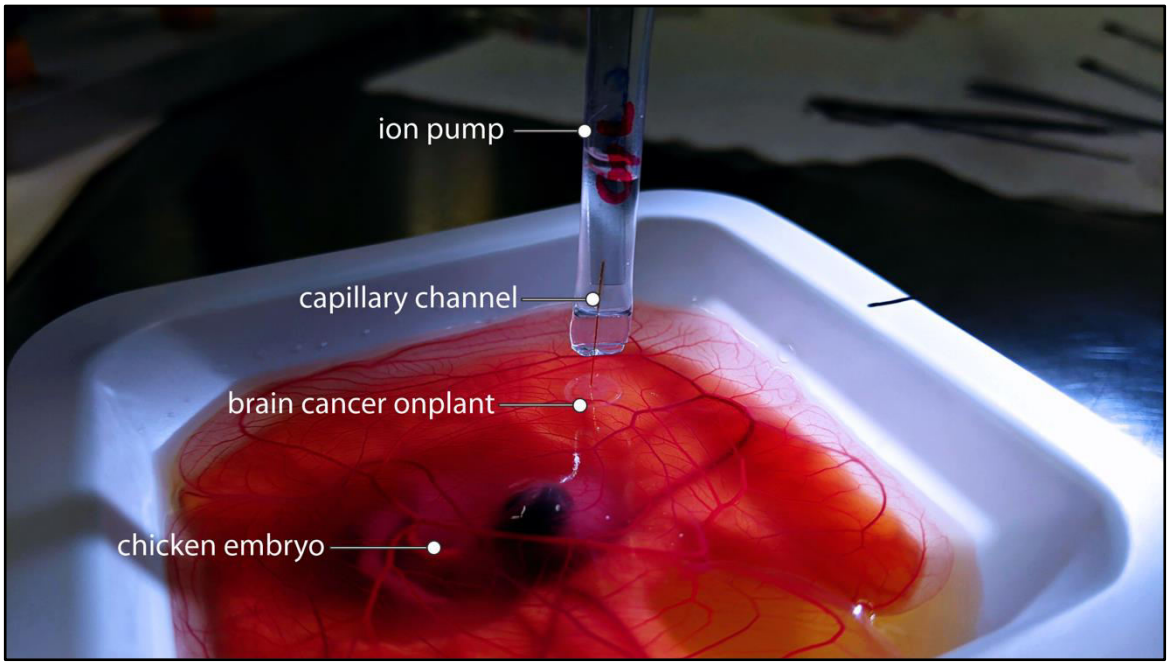

Figure 11: A detailed presentation of a GemIP inserted on the CAM of a chicken embryo. (kindly provided by L. Waldherr, personal communication – February 9th, 2021)

Subsequently, the xenografted chicken embryos were cultivated one last time for about 72 hours in the same setting as before. The day of harvest was marked by day 14 in our timetable – therefore, ‘1d after seeding‘ and ‘72h before harvesting‘ describe the same date but due to comparison reasons (e.g., 72h OR 30min before) a different choice of words was used.

The following tables present an overall view of the chicken embryos included as specimen for this thesis, their respective treatment condition with additional information as well as the time of application and the number of xenografted onplants. Chicken embryos which deceased within the implementation of the experiment are marked by a cross symbol (†). In order to prevent any confusion, the counting of the chicken embryos starts with the digit #1 at the beginning of a new year again – therefore, the first table sets up with #497 (2020) and the following ones go on with #175 (2021).

Table 2: Assay Setup for CAM #166 (seed. = seeding)

Specimen	*Condition*	*Onplant(s)*	*Info*	*Application*
497	GemIP	1	100mM/pH4	1d after seed.
498	GemIP	1	100mM/pH4	1d after seed.
499 †	No treatment	2	/	/
500	No treatment	2	/	/
501 †	GemIP	0	/	1d after seed.
502	GemIP	0	/	1d after seed.
503	GemIP	0	/	1d after seed.
504	GemIP	0	/	1d after seed.

The mentioned specimens of CAM-Assay #166 in the previous table were ultimately not included as data for the evaluation of the proliferation rate as we used a slightly different build GemIP in this one. Nevertheless, their pictures taken under the microscope are serving to represent the nonspecific inflammatory response and as a great illustration of the tumor growth behaviour – these will be shown in the chapter results.

Table 3: Assay Setup for CAM #170 (seed. = seeding, harv. = harvesting, combined = Gem manual + radiation; Gy = Grey)

Specimen	*Condition*	*Onplant(s)*	*Info*	*Application*
175	Gem manual	2	1µM	1d after seed.
176	Gem manual	2	1µM	1d after seed.
177	Gem manual	2	1µM	1d after seed.
178	Gem manual	2	1µM	1d after seed.
179	No treatment	2	/	/
180	No treatment	2	/	/
181	No treatment	2	/	/
182	Gem manual	2	1µM	4h before harv.
183	Gem manual	2	1µM	4h before harv.
184	Gem manual	2	1µM	4h before harv.
185	Radiation	2	10Gy	30min before harv.
186 †	Radiation	2	10Gy	30min before harv.
187	Radiation	2	10Gy	30min before harv.
188	combined	1	1µM/10Gy	4h/30min before harv.
189	combined	1	1µM/10Gy	4h/30min before harv.
190	combined	1	1µM/10Gy	4h/30min before harv.
191	combined	1	1µM/10Gy	4h/30min before harv.
192	combined	1	1µM/10Gy	4h/30min before harv.

Table 4: Assay Setup for CAM #171 (seed. = seeding, harv. = harvesting, combined = Gem manual + radiation; Gy = Grey; Cyt = Cytidine)

Specimen	*Condition*	*Onplant(s)*	*Info*	*Application*
194	GemIP	1	100mM/pH4	1d after seed.
195 †	GemIP	1	100mM/pH4	1d after seed.
196 †	GemIP	1	100mM/pH4	1d after seed.
197	GemIP	1	100mM/pH4	1d after seed.
198	CytIP	1	100mM/pH4	1d after seed.
199	CytIP	1	100mM/pH4	1d after seed.
200 †	CytIP	1	100mM/pH4	1d after seed.
201	CytIP	1	100mM/pH4	1d after seed.
202	CytIP	1	100mM/pH4	1d after seed.
203	Cyt manual	2	1µM	1d after seed.
204	Cyt manual	2	1µM	1d after seed.
205	Cyt manual	2	1µM	1d after seed.
206 †	†	2	/	/
207	Gem manual	2	1µM	1d after seed.
208	Gem manual	2	1µM	1d after seed.
209	Gem manual	2	1µM	1d after seed.
210	No treatment	2	/	/
211	No treatment	2	/	/
212 †	combined	1	1µM/10Gy	72h before harv.
213	combined	1	1µM/10Gy	72h before harv.
214	combined	1	1µM/10Gy	72h before harv.
215	combined	1	1µM/10Gy	72h before harv.
216 †	combined	1	1µM/10Gy	72h before harv.
217	Radiation	1		72h before harv.
218	Radiation	1		72h before harv.
219	Radiation	1		72h before harv.

220 †	Radiation	1		72h before harv.
221 †	Radiation	1		72h before harv.
222	combined	1	1μM/10Gy	4h/30min before harv.
223	combined	1	1μM/10Gy	4h/30min before harv.
224	combined	1	1μM/10Gy	4h/30min before harv.
225	combined	1	1μM/10Gy	4h/30min before harv.
226 †	combined	1	1μM/10Gy	4h/30min before harv.
227	combined	1	1μM/10Gy	4h/30min before harv.
228 †	†	1	/	/
229	Radiation	1	10Gy	30min before harv.
230	Radiation	1	10Gy	30min before harv.
231	Radiation	1	10Gy	30min before harv.
241 †	GemIP	1	100mM/pH4	1d after seed.
242	Radiation	1	10Gy	72h before harv.
243	Radiation	1	10Gy	30min before harv.
244	Radiation	1	10Gy	30min before harv.
245	No treatment	1	/	/
246	No treatment	1	/	/
247	No treatment	1	/	/

3.2.2.3 Harvest and paraffin embedding

Once the last 72 hours in the incubator had passed (day 14), the graft containing silicon rings were excised using a surgical scissor and tweezers. The removed rings then were put in small and labeled petri dishes filled with 1X Phosphate-buffered saline (PBS) each. To reduce the risk of extensive bleedings as a result of accidently bruised blood vessels but also to slow down the chicken embryo's metabolism almost to a standstill, the embryos were stored in an ice filled container for a brief period at first. For the acquisition of initial data regarding the tumor growth behavior after the different handling, pictures of both the upper and lower surface of each silicon ring were captured by the computer software cellSense using a stereo microscope. As last step of the day, the rings were transferred from the PBS-dishes into petri dishes filled with 4% paraformaldehyde (PFA) – where they remained overnight at the normal environmental temperature.

On the following day, the formalin fixation of the excised tumor rings came next: In order to allow a smooth fixation process, the xenografted rings were firstly placed in Tissue-Tek® cassettes prior to draining the tissue in an ascending alcohol series according to an established concept (a detailed description is shown in Table 2).

In a last step, two days after the fixation process the paraffin embedding followed. After carefully separating the xenografted tumor tissue from the silicon rings with the help of tweezers, a Tissue-Tek® cassette corresponding mold was used to embed the tissue. A noteworthy aspect to the embedding process is that the tissue was embedded in a plane perpendicular to the cassette's bottom – by this way a histological sectioning in multiple slides along the entire extent of the tumor tissue is granted. The finished paraffin blocks were then stored securely at 4°C right after a brief moment on a cooling plate (-15°C).

Table 5: Fixation concept (all steps at environmental temperature)

Substance	*Percentage*	*Time-Period*
Ethanol	70%	30min
Ethanol	95%	30min
Ethanol	95%	15min
Ethanol	100%	30min
Ethanol	100%	15min
Toluene	/	30min
Toluene	/	15min

3.3 Histology

To be able to quantify the effects of the GemIP on the proliferation rate of the C6 rat GBM cells in relation to the otherwise treated C6 cells, a histological sectioning and immunohistochemical staining of all C6 cell line samples was required. The immunostaining aimed for a specific protein called Ki-67 as antigen.
The expression of Ki-67 is a prominent marker for the investigation of cell proliferation [23]. In particular, the Ki-67 protein is expressed immensely in tumor cells and can consequently be utilized as predictive and prognostic indicator for cancer progression [24]. As a marker, the Ki-67 expression is considered for various tumor types including GBM – a distinct Ki-67 staining pattern is related to high proliferation rate and poor prognosis according to several studies [25].

3.3.1 Sectioning

With a rotary microtome tissue sections of 5µm thickness were prepared on Thermo Scientific™ SuperFrost Plus object slides – these special object slides had the purpose of minimalizing the risk of tissue los; on each slide we put several cohesive sections, to fill almost the entire length of the slide. The section containing slides were then immersed briefly in a 38°C warm water bath (distilled water) to stretch and straighten the cohesive sections before being set down on a heating plate (38°C) to evaporate the remaining humidity.

3.3.2 Immunohistochemical staining

The staining followed a specific 2-day protocol, which is displayed in the table below in all details. As already mentioned, the Ki-67 expression is an indicator for proliferation and therefore the associated protein our targeted antigen. Corresponding primary antibodies were used to bind explicitly to the stated Ki-67 protein and in a next step, a secondary antibody was added to the histological preparations. The secondary antibody is directed at the primary antibody; their interaction generates the desired and easy visible color change in strongly expressing cells. This task was later kindly performed by the Institute of Pathology (MedUni Graz) by reasons of availability of specialized tools for the staining – allowing them to stain multiple slides simultaneously in a shorter period of time.

Table 6: Immunostaining protocol (TBS-T = Tris-buffered saline + Polysorbate 20)

Step	*Substance*	*Duration*	*Repeats*	*Add. Info*
Day 1				
Deparaffinization	RotiClear	10min	2x	/
	Xylol: EtOH	5min	2x	100% EtOH
	EtOH	3min	2x	1. 95%, 2. 70%
	Aqua dest.	3min	2x	/
Decloaking Chamber	heating up	40min	1x	95°C
	cooling down	10min	1x	/
	Aqua dest.	5min	2x	/
Day 2				
Antibody	POX Block	apply (10-25min)	1x	Hydrogen Peroxidase Block
	TBS-T Wash	5min	4x	/
	Protein Block	apply (5-20min)	1x	Ultra-V Block
	TILT			
	1st Antibody	apply	1x	diluted 100µL/sample
	TBS-T Wash	5min	4x	/
	Enhancer	apply	1x	(10min)
	TBS-T Wash	5min	4x	/
	Polymer HRP	apply	1x	(15min)
	TBS-T Wash	5min	4x	/
	Chromogen	~2min	1x	Aec + DAKO
	Aqua dest.	5min	4x	/
Counterstaining	Hemalum	12sec	1x	Mayer's solution
	Aqua dest.	5min	4x	/
	Ammonium Hydroxide	dips	~10x	2.5ml per 1L
	Aqua dest.	5min	4x	/
	Aqua dest.	cover	1x	keep moist

The immunohistochemical staining allows a division of the tumor cells in two groups depending on the intensity of their nuclear staining: Ki-67 positive cells (brown) and Ki-67 negative cells (blue). This classification forms the basis of the so-called Ki-67 proliferation index – an index introduced to enable a quantitative comparison of proliferation rate between individual immunostained histological slides.

The Ki-67 proliferation index is displayed in percentages (0-100%) and defined as total count of Ki-67 positive tumor cells divided by total count of all tumor cells in each field/image with the result being multiplied by a factor of 100 [26]. Hence, a stereo microscope captured and stored high-resolution digital images in 400-fold magnification using a specialized software. Another for this purpose provided software counted Ki-67 positive cells as well as the total number of tumor cells and calculated the Ki-67 proliferation index automatically for us. In each digital image, the software randomly picked high-power fields to calculate the Ki-67 index – these are the results, which ultimately entered the statistical evaluation and represent the findings of this thesis.

4. Results

For this thesis, the effects of a GemIP on the proliferation rate of Glioblastoma C6 rat cells were investigated as part of a larger research project. As the previous section gave a detailed insight into the experimental protocol, the following chapter will reveal our obtained findings. Additionally, the study analysis and statistical evaluation should provide a guidance for further steps in the research project and the ultimate aim of designing a drug delivering IP for clinical trials.

4.1 Growth behaviour and tumor formation

The C6 GBM cell line showed a great growth behavior on the CAM, forming solid and well-demarcated tumor masses. Naturally, slight differences were visible in the morphology and growth behavior of the masses according to their respective treatment condition. In embryos #497-500 we took pictures of the silicon ring directly on the CAM on day of onplant implantation and three days later; followed by taking images of the bottom and top side of the excised rings on the same day. The rings of the remaining embryos were only pictured three days after onplant implementation, directly on the CAM as well as bottom and top side after excision. The illustrations beneath present the tumor growth on the CAM and on the excised xenografts of one selected embryo as a representative example for each treatment.

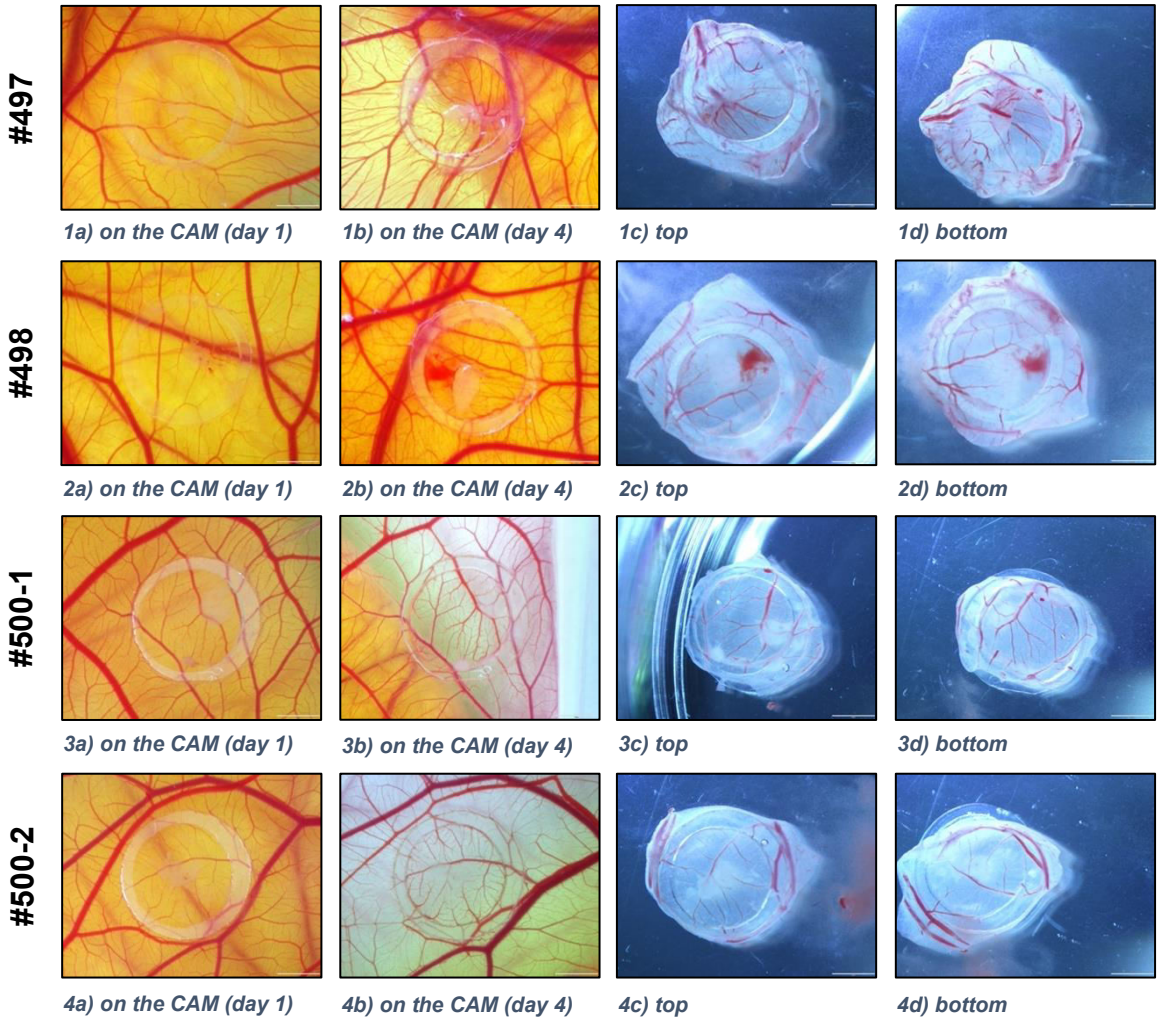

Figure 12: Representative pictures of the tumor growth behavior taken under the microscope – on day of implementation (a), three days later (b) and after excision (c, d). #497/498 -> GemIP 1d after seeding, #500 -> No treatment.

As the tumor formation was already visible to the naked eye and due to unavailability of a microscope, the xenografted and then excised onplants in CAM #170 (Fig. 13) and in CAM #171 (Fig. 14) were pictured macroscopically using a normal lens without magnification. However, the images in Fig. 12 serve to demonstrate the tumor formation and growth behavior on a more microscopical scale – these subjects were not taken in consideration to determine the Ki-67 proliferation index and were only used for the purpose of illustration at this point.

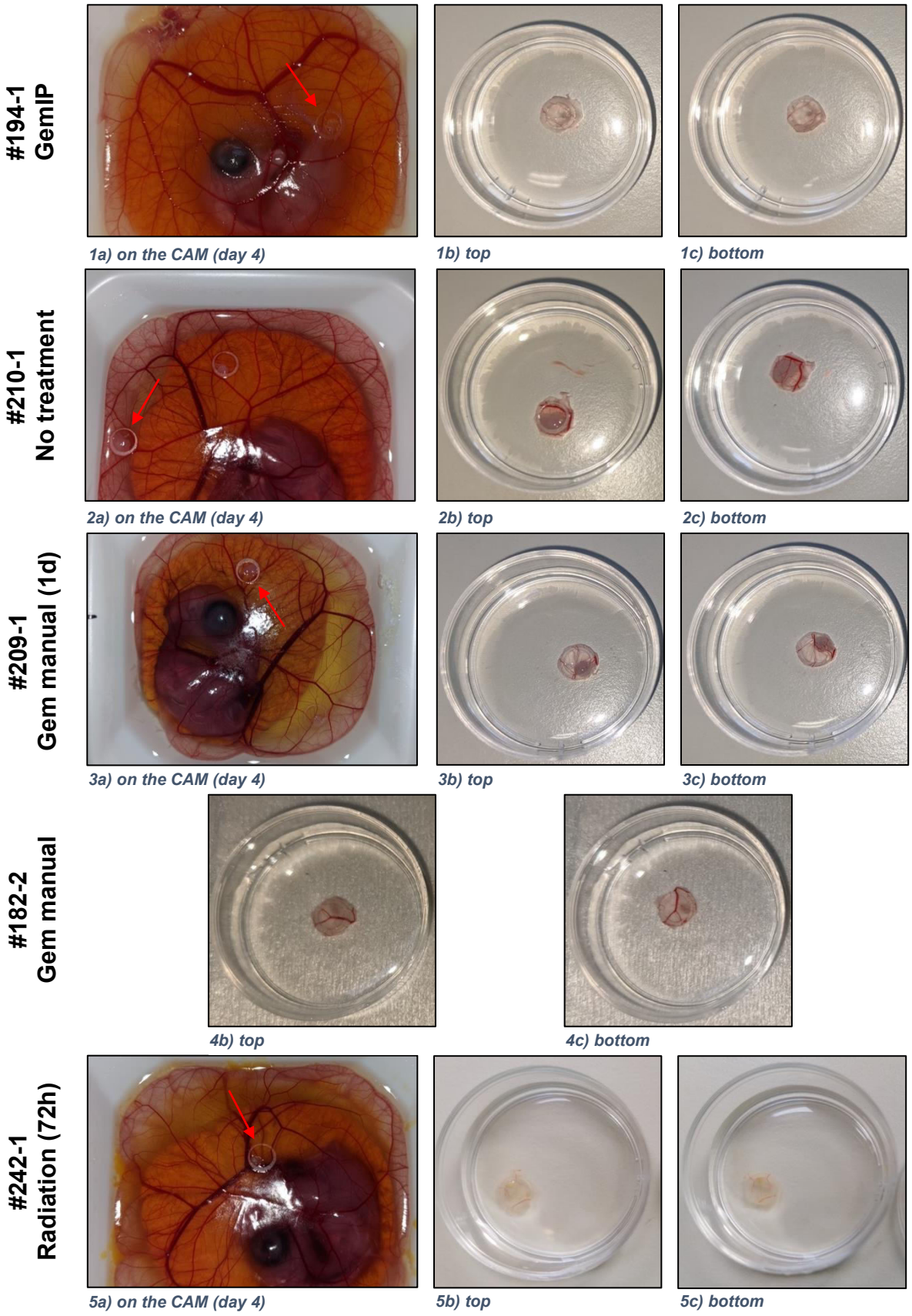

Figure 13: Representative pictures of the macroscopic visible tumor for each treatment condition – before (a) and after (b, c) excision of the onplant. The red arrows point out the xenografted onplants on the CAM. #194 -> GemIP 1d after seeding, #210 -> No treatment, #209 -> Gem manual 1d after seeding, #182 -> Gem manual 30min before harvesting, #242 -> Radiation 72h before harvesting.

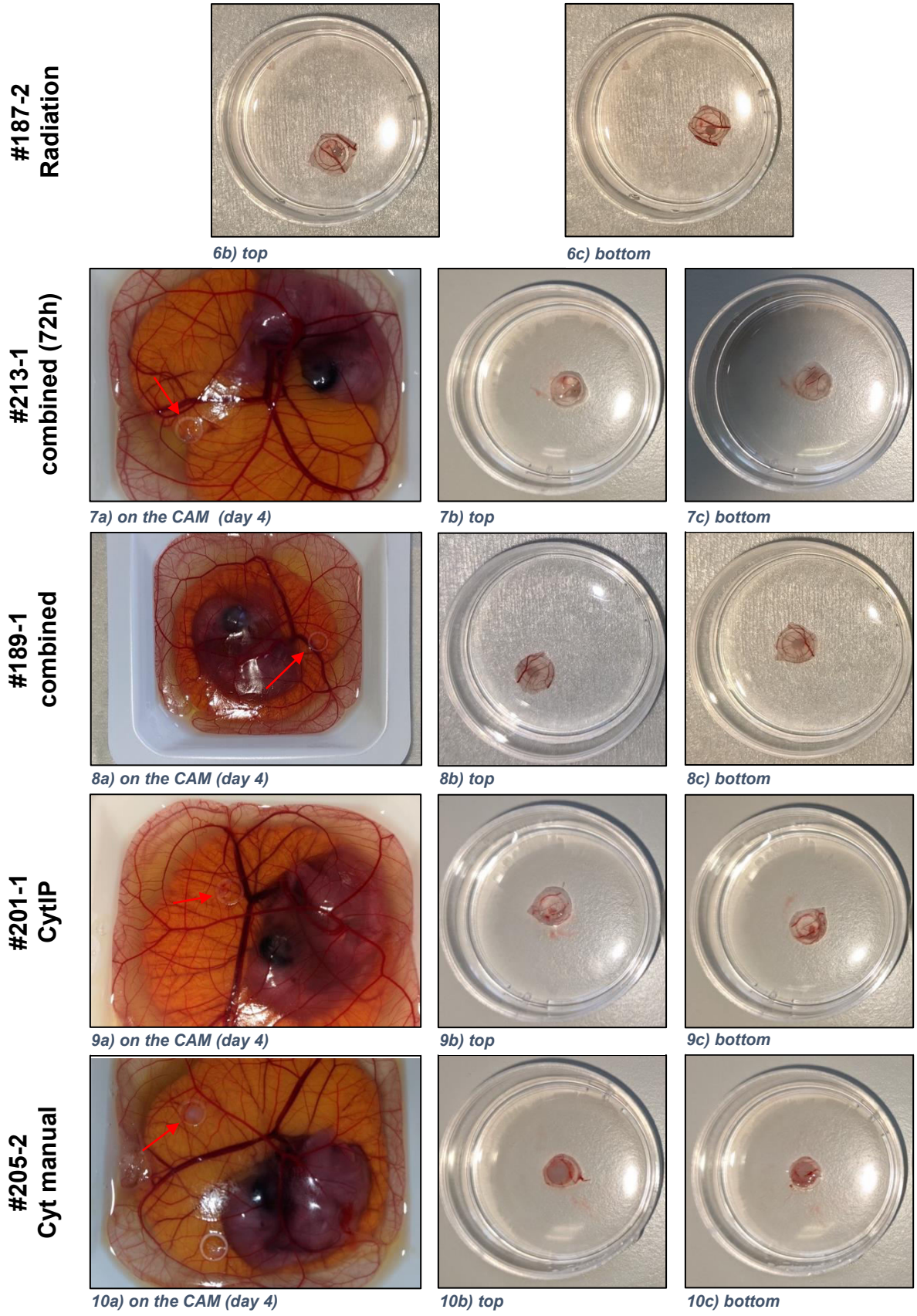

Figure 14: Representative pictures of the macroscopic visible tumor for each treatment condition – before (a) and after (b, c) excision of the onplant. The red arrows point out the xenografted onplants on the CAM. #187 -> Radiation 30min before harvesting, #213 -> combined treatment 72h before harvesting, #189-> combined tr. 4h/30min before harvesting, #201 -> CytIP 1d after seeding, #205-> Cyt manual 1d after seeding.

As already mentioned, a nonspecific inflammatory response is the main limitation of the CAM model [10] – by piercing the surface of the CAM with a GemIP, an inflammatory reaction was to be expected. To be able to document the total extent of the reaction caused by the said process, samples #501-504 have been manipulated with GemIPs alone; no onplants, no tumor cells.

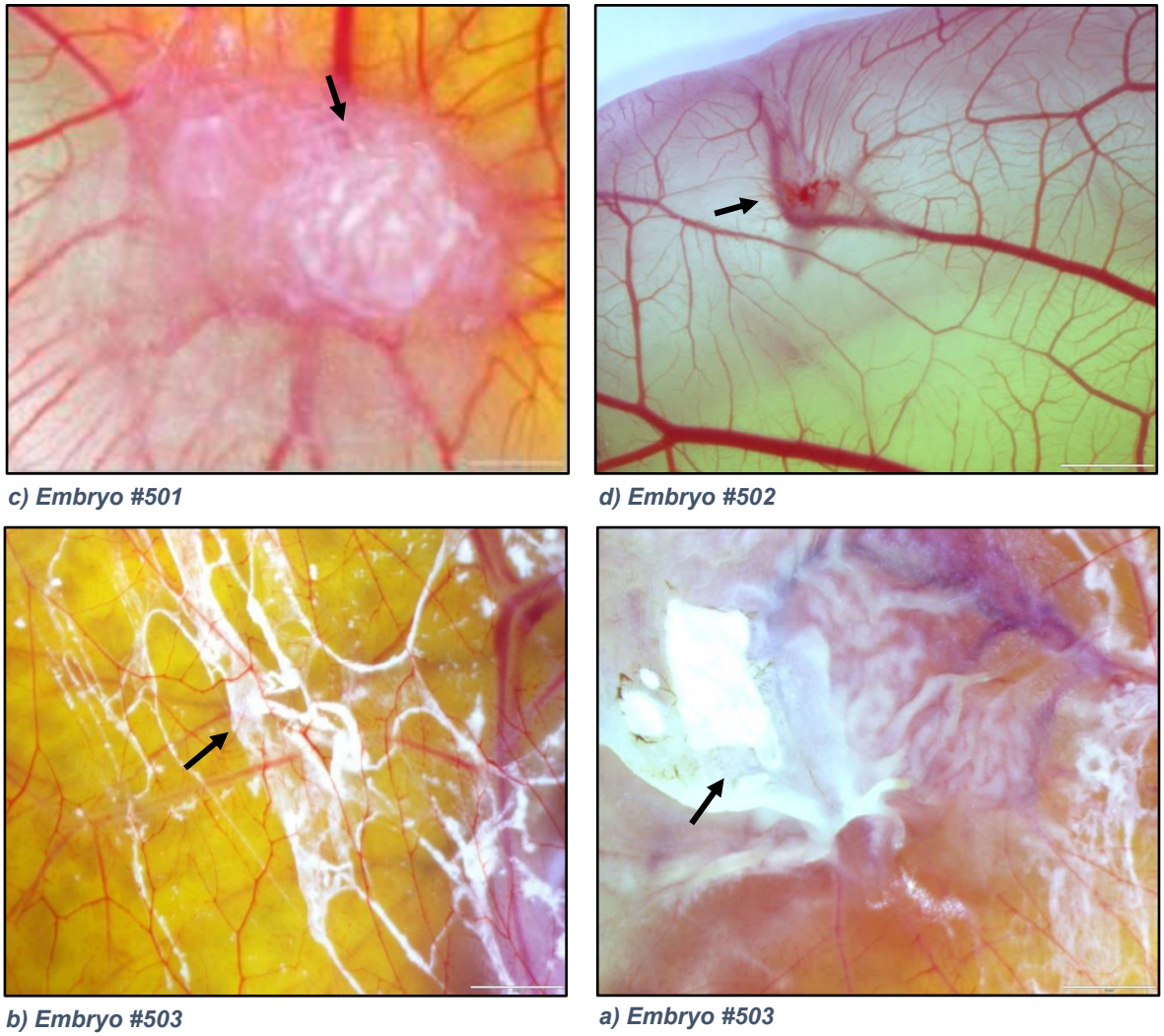

c) Embryo #501

d) Embryo #502

b) Embryo #503

a) Embryo #503

Figure 15: Nonspecific inflammatory response – these images were taken under the microscope three days after insertion of the GemIP, showing clear signs of an inflammatory process (arrows). Fig. 11a): usual response. Fig. 11b): only minimal changes visible, most probably due to lacking contact between GemIP and surface. Fig. 11c)/d): display the massive response in sample #503.

4.2 Histological analysis

For the evaluation of the experimental results in terms of efficiency of the GemIP on the proliferation rate in the C6 GBM rat cell line, the following passage will summarize our data acquired by the histological analysis of the paraffin embedded tissue.

4.2.1 Hematoxylin and eosin (HE) staining

Regarding the determination of proliferation rate and Ki-67 index, a H&E staining is not required and thus not a necessity to evaluate the experimental results in that respect. As a matter of routine, a staining wit HE is always performed in one portion of available histological sections for each of our CAM assay runs – this method provides a general overview of a sample's structure, layout and cell distribution by staining various tissue constituents [27]. In the interests of completeness, the subsequent figures will serve as a representative example to present the histological morphology of a xenografted onplant – and additionally outline the slight difference in histological tumor morphology of an untreated (Fig. 16) and a treated (Fig. 18) onplant.

In order to ensure the most appropriate slides are chosen for the Ki-67 staining, the tissue sections of each paraffin block were stained with H&E in steps of five – starting with the first slide: #1, #5, #10 etc.
This approach allowed us to determine the tissue sections which have caught the largest tumor expansion for each paraffin block and thus use adjacent slides for the determination of the Ki-67 index – the procedure is exemplary displayed in Fig. 17 and Fig. 19.

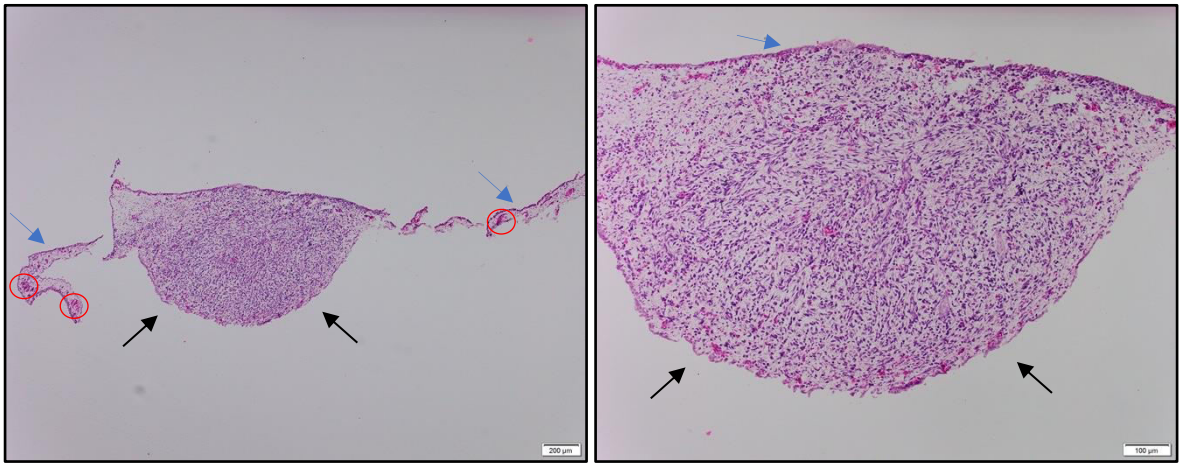

a) 4x magnification *b) 10x magnification*

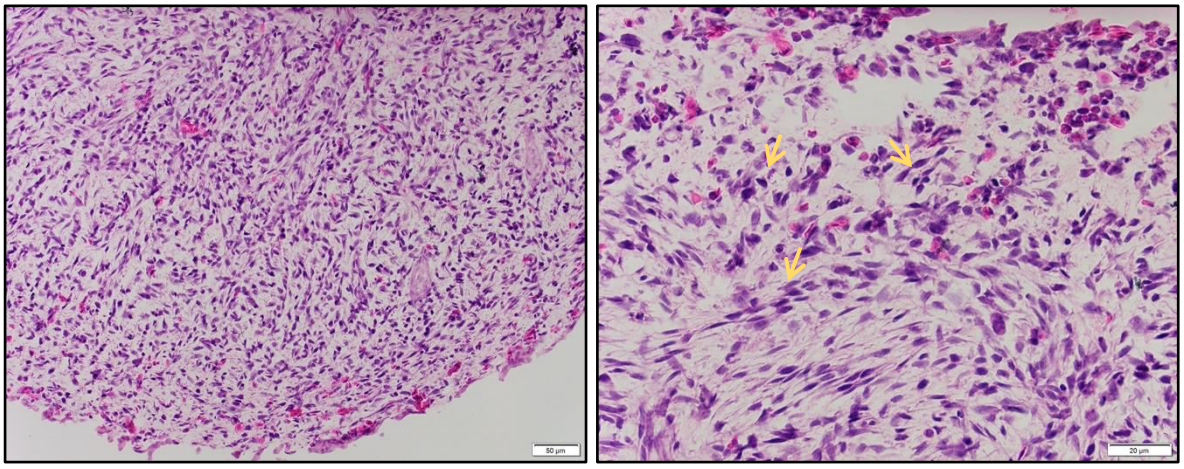

c) 20x magnification *d) 40x magnification*

Figure 16: Representative example for a H&E staining of an untreated Onplant (#181_1) – displayed in different magnifications (a-d) to highlight the important characteristics of a xenograft: the xenografted tumor (black arrows), the CAM (blue arrows), blood vessels (red rings) and hyperchromasia/mitotic figures as a typical criterion for malignancy (yellow arrows).

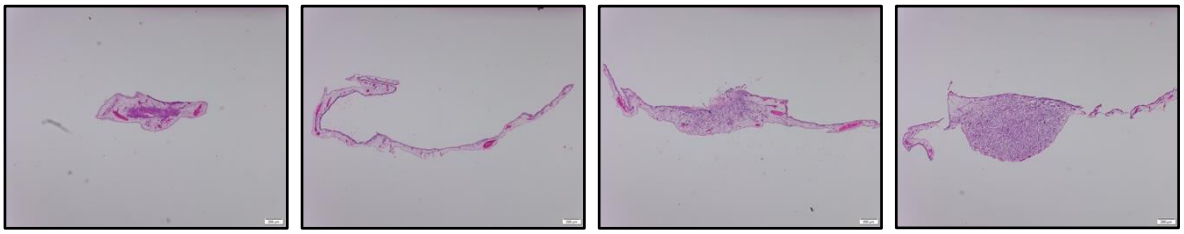

a) Slide #1 *b) Slide #5* *c) Slide #10* *d) Slide #20*

Figure 17: Sequence of the sectioned and stained tissue of onplant #181_1 in 4x magnification. Fig. 17a) and 17b): only CAM visible. Fig. 17c): beginning tumor growth. Fig. 17d): maximal detected tumor expansion.

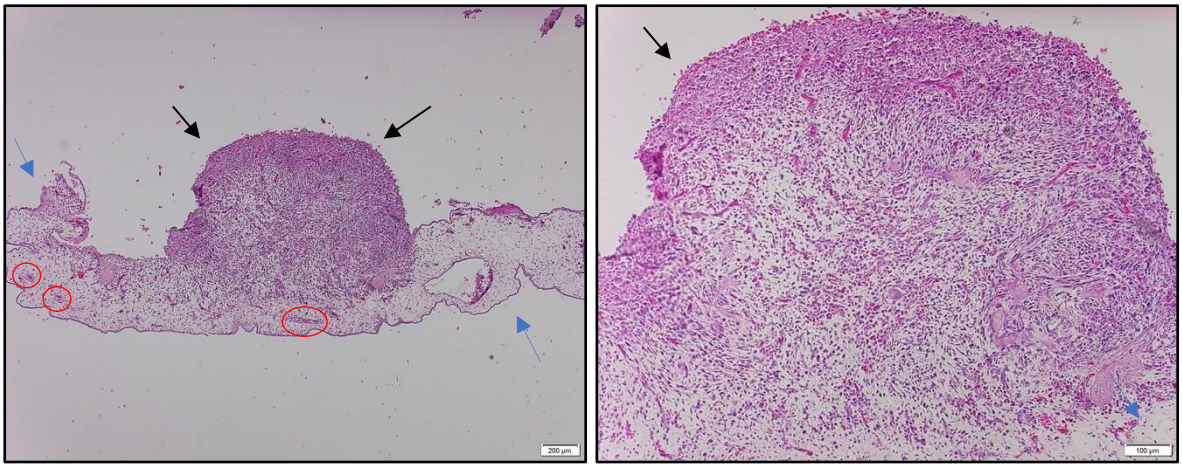

a) 4x magnification *b) 10x magnification*

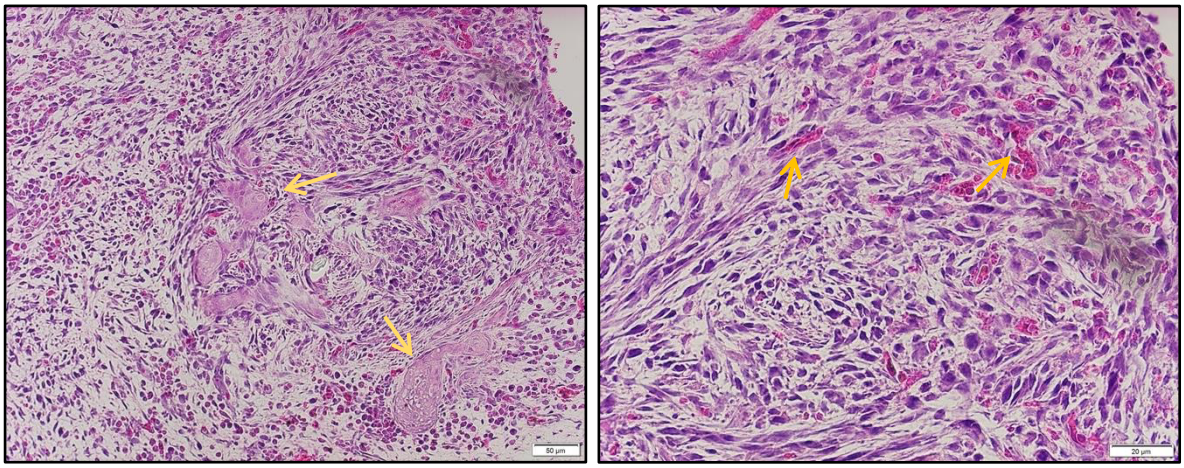

c) 20x magnification *d) 40x magnification*

Figure 18: Representative example for a H&E staining of a treated Onplant (#197_1) – displayed in different magnifications (a-d) to highlight the important characteristics of a xenograft: the xenografted tumor (black arrows), the CAM (blue arrows), blood vessels (red rings), necrosis -characterized by loss of the cell nucleus (yellow arrows) - and stronger eosinophilic color of the cells as a typical sign of progressive degeneration (orange arrows).

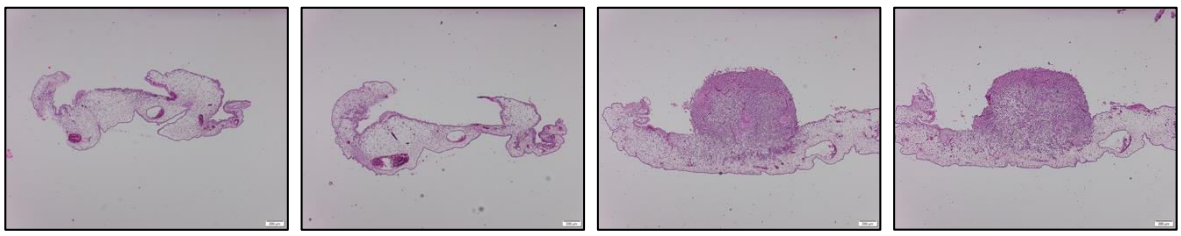

a) Slide #5 *b) Slide #10* *c) Slide #15* *d) Slide #20*

Figure 19: Sequence of the sectioned and stained tissue of onplant #197_1 in 4x magnification. Fig. 17a) & 17b): only CAM visible. Fig. 17c) & 17d): maximal detected tumor expansion.

4.2.2 Ki-67 Index

This chapter will expound our results regarding the determination of the proliferative index Ki-67 for the differently treated samples. The chosen tissue slides were immunohistochemically stained, high-resolution images prepared and suitable magnifications for quantitative assessment selected. To exemplify the principle of the Ki-67 staining, Fig. 20 below will function as a representative image for illustrative purposes.

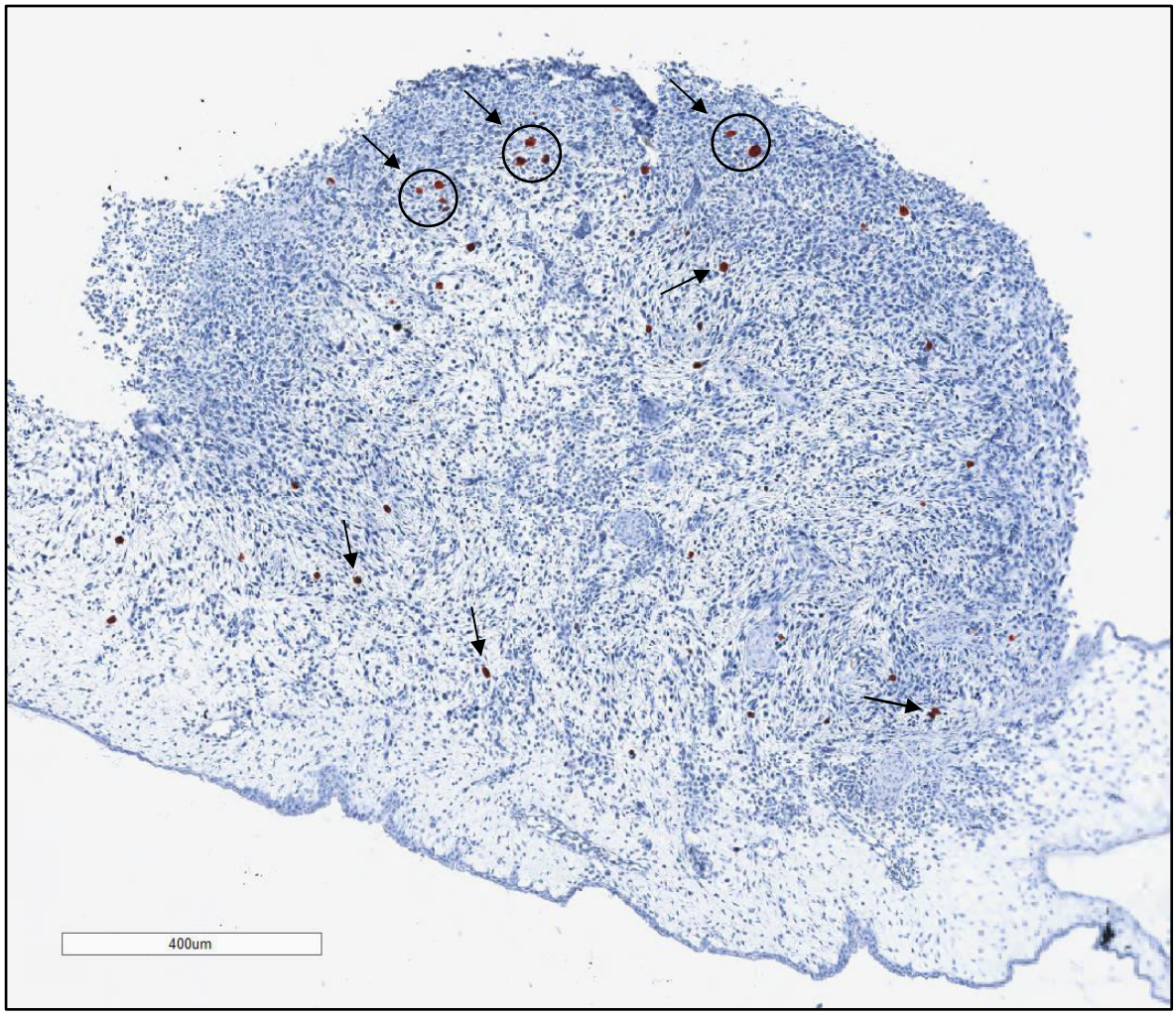

Figure 20: Representative example of an immunohistochemical staining for Ki-67 (image scale: 400µm, Onplant #197_1, Slide #19). „Positive" cells are marked by black arrows – proliferating cells point out a strong expression of the marker Ki-67, which is responsible for the intense brown color of the rapidly dividing tumor cells. In contrast, „negative" cells are missing the intensive brown and show a bluish discoloration.

As Fig. 20 gave an exemplary description of this immunostaining variant, the following will display the received staining outcome for each treatment condition.

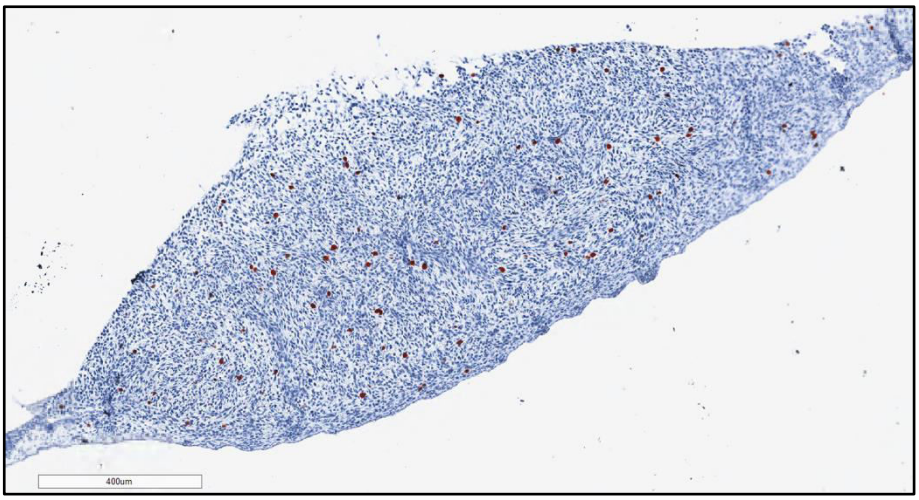

a) Onplant #210_2, Slide #18, image scale: 400µm – No treatment.

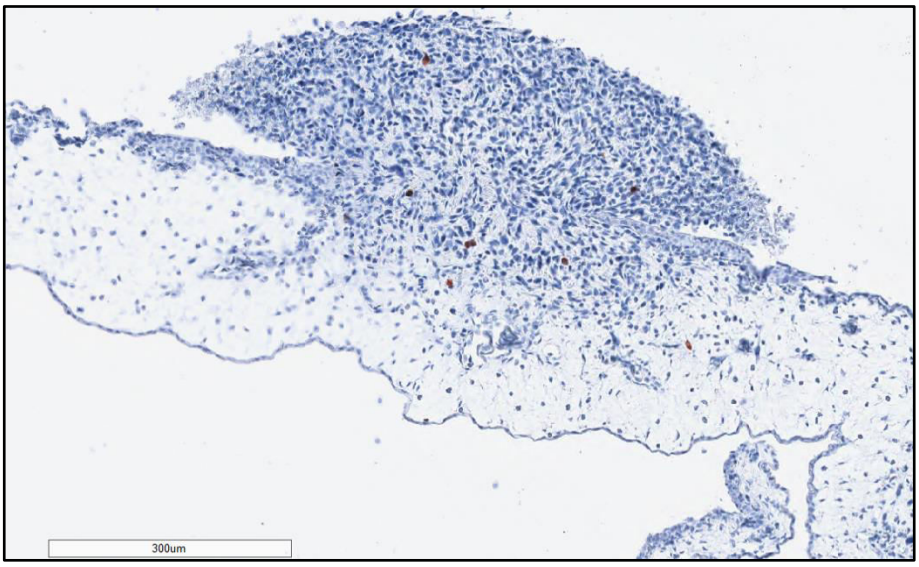

b) Onplant #184_1, Slide #16, image scale: 300µm – Gem manual (4h before harvesting).

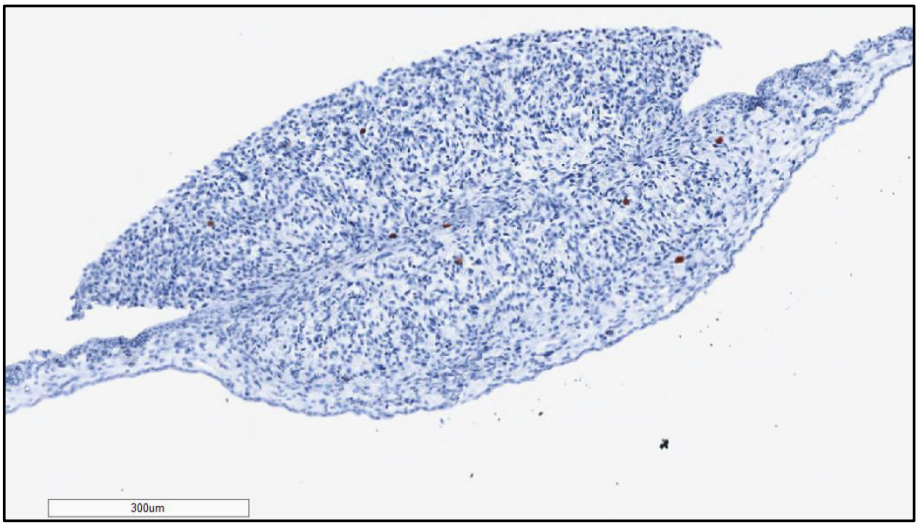

c) Onplant #185_1, Slide #16, image scale: 300µm – Radiation (30min before harvesting).

Figure 21: Results (1/3) of the immunohistochemical staining Ki-67 for different treatment conditions.

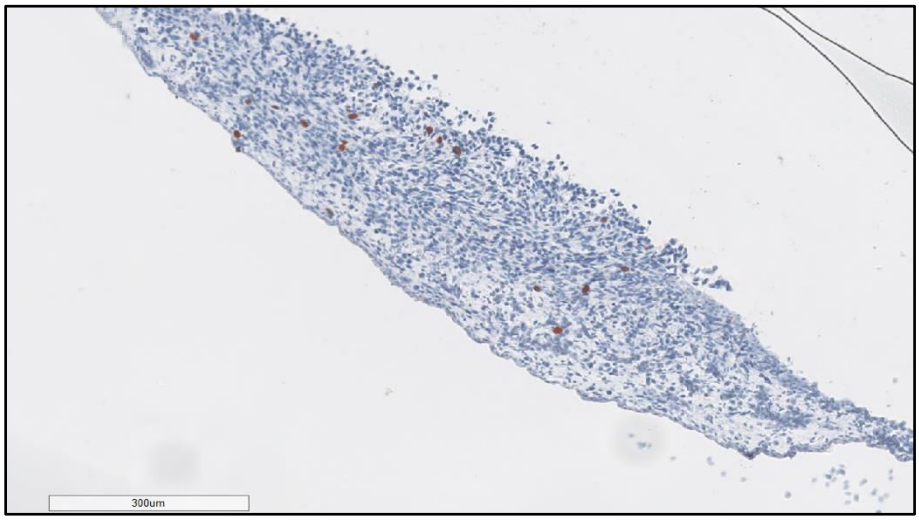

a) Onplant #190_1, Slide #12, image scale: 300µm – combined th. (4h/30min before harv.).

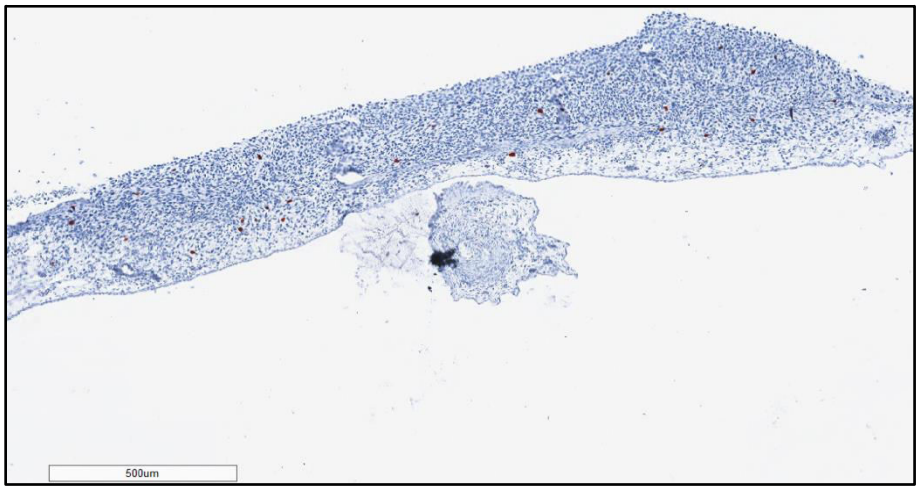

b) Onplant #194_1, Slide #6, image scale: 500µm – GemIP.

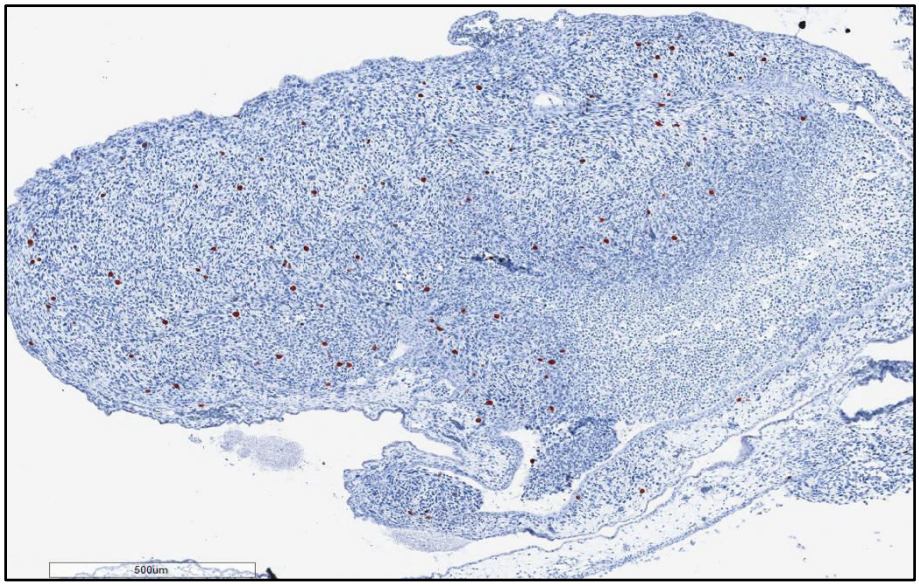

c) Onplant #199_1, Slide #16, image scale: 500µm – CytIP.

Figure 22: Results (2/3) of the immunohistochemical staining Ki-67 for different treatment conditions.

The

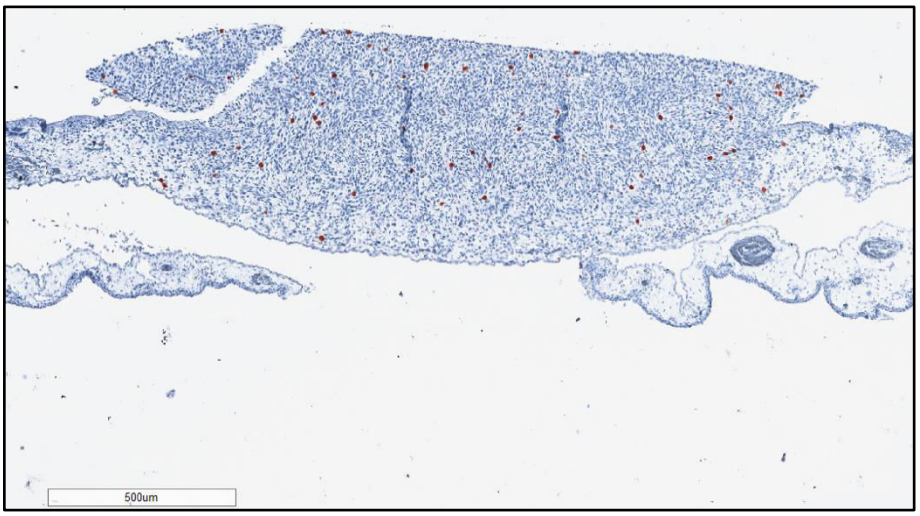

a) Onplant #205_2, Slide #6, image scale: 500µm – Cyt manual.

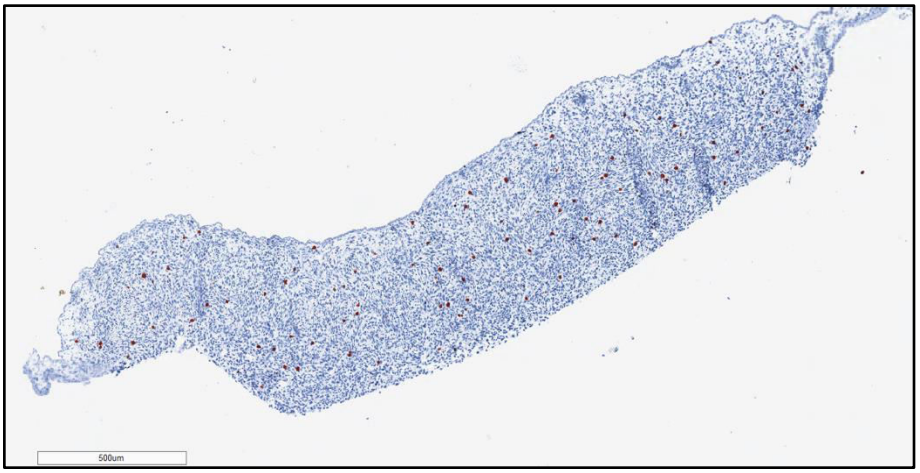

b) Onplant #208_2, Slide #19, image scale: 500µm – Gem manual (1d after seeding).

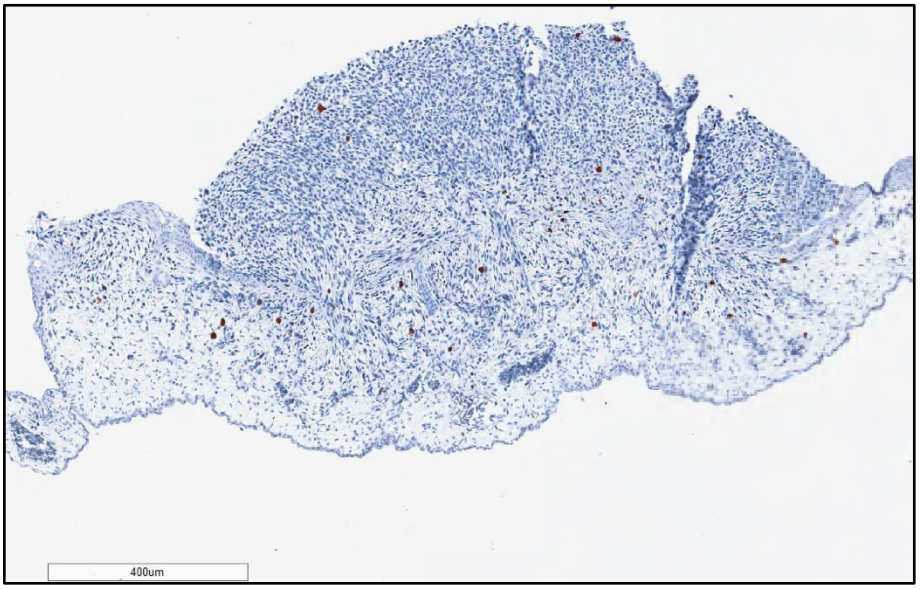

c) Onplant #215_1, Slide #19, image scale: 400µm – combined th. (72h before harvesting).

Figure 23: Results (3/3) of the immunohistochemical staining Ki-67 for different treatment conditions.

immunohistochemical stained slides served as foundation for the calculation of the proliferation index Ki-67. Therefore, the software „QuPath" was used – enabling whole slide image analysis. The software allows the user to define „positive" (brown) as well as „negative" (blue) depending on the intensity of the cell's nuclear staining at one's own discretion. The subsequent table presents the total number of detected cells, the number of negative/positive cells and the thereof determined Ki-67 index for all the slides selected by us.

Table 7: The proliferation index Ki-67 (Data acquired by the software QuPath)

Specimen	*Slide*	*Detections*	*Negative*	*Positive*	*Ki-67 (%)*
181_1	19	8566	8520	46	**0,537**
182_2	16	793	792	1	**0,1261**
184_1	16	2463	2455	8	**0,3248**
185_1	16	3996	3987	9	**0,2252**
187_2	16	591	590	1	**0,1692**
189_1	16	1223	1222	1	**0,0818**
190_1	12	2824	2786	38	**1,346**
191_1	12	5917	5905	12	**0,2028**
194_1	6	7839	7792	47	**0,5996**
197_1	19	13264	13206	58	**0,4373**
198_1	6	6645	6606	39	**0,5869**
199_1	16	26397	26251	146	**0,5531**
203_2	16	12744	12637	107	**0,8396**
204_1	6	9853	9728	125	**1,269**
205_2	6	9911	9825	86	**0,8677**
207_1	19	6179	6142	37	**0,5988**
208_2	19	14267	14121	146	**1,023**
210_2	1	13761	13715	46	**0,3343**
210_2	6	/	/	/	/

210_2	10	13985	13963	22	**0,1573**
210_2	12	9452	9377	75	**0,7935**
210_2	18	12047	11926	121	**1,004**
210_2	19	12166	12091	75	**0,6165**
210_2	19-002	3437	3425	12	**0,3491**
210_2	19-003	3676	3657	19	**0,5169**
211_2	2	15401	15346	55	**0,3571**
211_2	11	/	/	/	/
211_2	17	14261	14187	74	**0,5189**
213_1	19	10429	10394	35	**0,3356**
214_1	19	19258	19167	91	**0,4725**
215_1	19	9382	9337	45	**0,4796**
(Spleen)	11	2931	2613	318	**10,85**

The presented indices reflect the results of the remaining proliferation rate after the specimens' respective treatment condition. In addition, in order to aid visualization and a better comparison, the said values are represented graphically in Fig. 24 and Fig. 25 below. Whereas Fig. 24 only displays the results for chemo treatment, the following Fig. 25 adds the (chemo-)radiation one's as well – this conscious separation should provide an even better overview of the outcome. Besides the individual values of the Ki-67 index results, the illustrations also depict the mean value for the indices of each treatment condition.

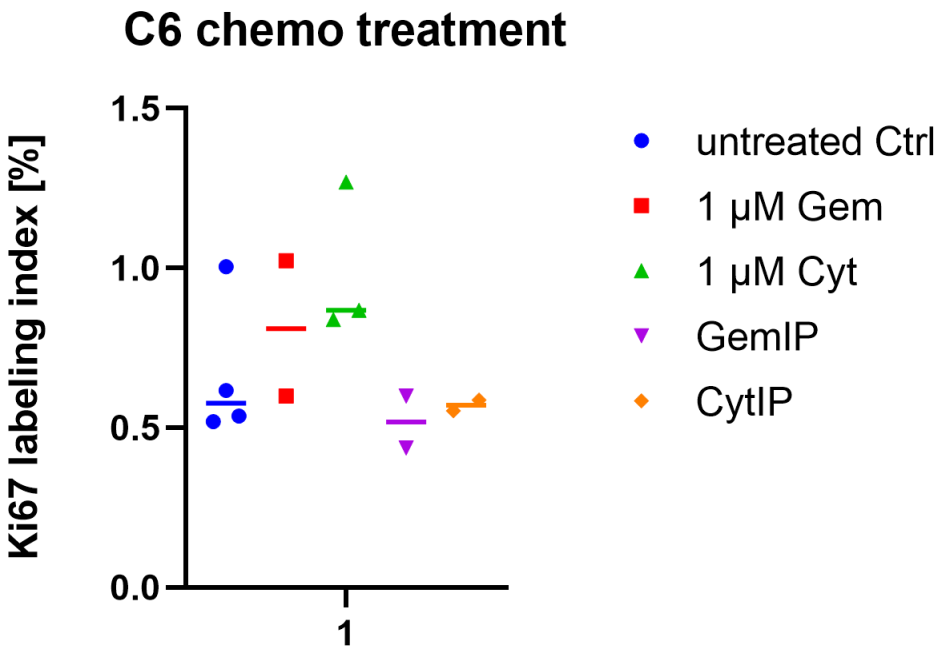

Figure 24: Ki-67 index for samples treated with chemo – single values and mean value.

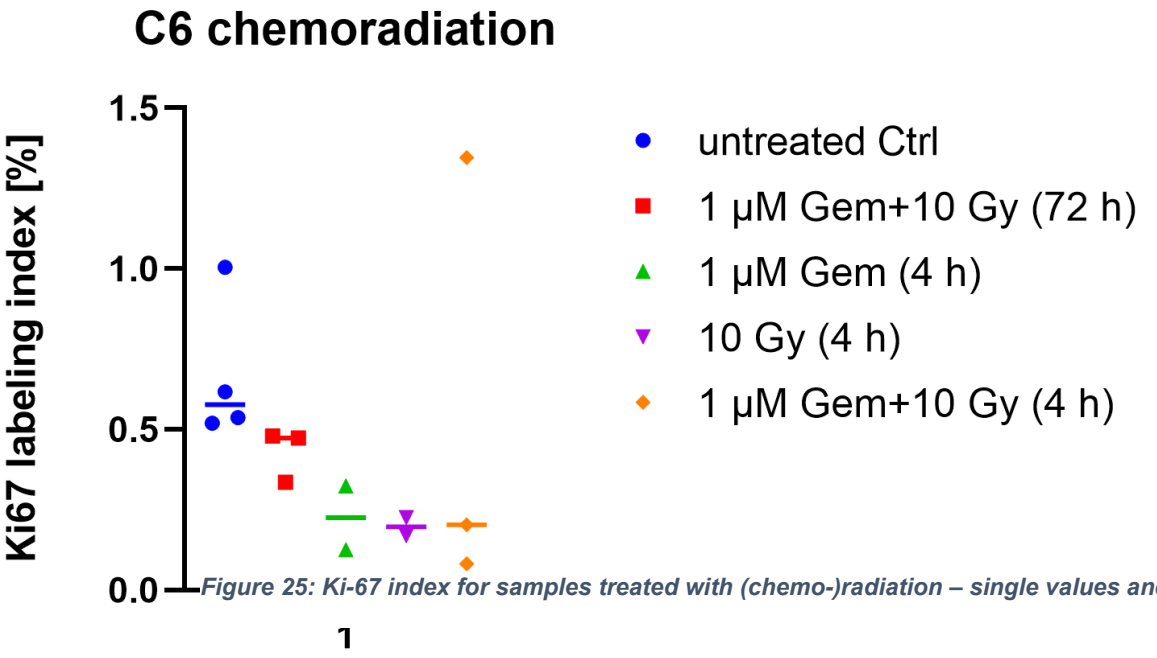

Figure 25: Ki-67 index for samples treated with (chemo-)radiation – single values and mean value.

5. Discussion

The WHO grade IV GBM is a by rapid growth and a diffuse invading-pattern characterized brain neoplasm which shows low sensitivity to radio- and chemotherapy [1]. The current state-of-the-art approach for the complex and heterogenic tumor is a multimodal therapy concept including maximal safe surgical removement followed by a combination of radio- and chemotherapy [5].
Yet, the GBM shows a high rate of reoccurrence and in most cases a progression to death within 12-18 months after diagnosis – making it one of the deadliest neoplasms in general. Despite his malignancy and frequency, neither overall survival nor prognosis could be significantly improved over the last decades [1].

The implementation of an iontronic pump in form of a drug delivery device after surgical intervention would not only bypass the blood-brain-barrier but also allow a precise local treatment of remaining GBM single cells.
The described study was conducted to evaluate the effectivity of an organic electronic ion pump as well as to optimize further steps in the research project.

It was possible to prove the functionality of an OEIP on C6-Glioblastoma cells with the conducted experimental series in this study. Regarding chemo treatment, the GemIP showed a slightly lower average Ki-67 index compared to the untreated or otherwise with chemo treatment treated C6 cells – including our positive control treated with Cytidine. In contrast, samples which were treated by radiation or chemoradiation showed a lower average Ki-67 index than the GemIP one's.
Without the involvement of radiation, the GemIP exhibits an increased effectivity compared to other treatment options. Unfortunately, the number of eventually usable and included samples was too small to name the results as clear or significant.

Nevertheless, the functionality of an organic electronic ion pump was proven by the experimental series. A very essential foundation for prospective phases of the research project was laid as for the next step, a transition from testing the GemIP in the CAM model to investigations on rats is planned – thereby rats with induced GBM are supposed to be treated by implanted GemIPs. Therefore, the evidence of GemIP effectivity on C6-Glioblastoma rat cells is another advantage for the following step in the project.

Naturally, the used OEIP is still a prototype and further test runs in the CAM model with various adjustments as well as upgrades are to follow. A possible combination of OEIP and radiation for maximization of therapeutic success in the treatment of GBM should be taken into consideration too, referring to the results of chemoradiation.

In conclusion, OIEPs and especially GemIPs are a suitable method for the treatment of C6-Glioblastoma rat cells. Even though this study was not able to present the desired significant results, at least the functionality and effectivity of a GemIP were proven in this model – along with a foundation for improvements in further research phases. There are still many experimental steps to take before going on the human body and establishing a revolutionary therapeutic approach. However, the conducted experimental series remains an important and inevitable study for the future in treatment of Glioblastoma Multiforme.

6. Bibliography

[1] Hayat MA. Tumors of the Central Nervous System, Volume 1: Gliomas: Glioblastoma. Netherlands: Springer Dordrecht Heidelberg London New York; 2011. p. 3-4.

[2] Rao JS. Molecular mechanisms of glioma invasiveness: the role of proteases. Nature Reviews Cancer. 2003;3(7):489-501.

[3] Taal W, Bromberg JE, Bent MJvd. Chemotherapy in glioma. CNS Oncology. 2015;4(3):179-192.

[4] Khosla D. Concurrent therapy to enhance radiotherapeutic outcomes in glioblastoma. Ann Transl Med. 2016;4(3):54.

[5] Somasundaram K. Advances in Biology and Treatment of Glioblastoma. Springer International Publishing AG; 2017. p. 57-62.

[6] Karachi A, Dastmalchi F, Mitchell DA, Rahman M. Temozolomide for immunomodulation in the treatment of glioblastoma. Neuro Oncol. 2018;20(12):1566-1572.

[7] Elmaci İ, Bilir A, Ozpinar A, Altinoz MA. Gemcitabine, vinorelbine and cyclooxygenase inhibitors in the treatment of glioblastoma. Ultrastructural analyses in C6 glioma in vitro. Tissue Cell. 2019;59:18-32.

[8] Bastiancich C, Bastiat G, Lagarce F. Gemcitabine and glioblastoma: challenges and current perspectives. Drug Discov Today. 2018;23(2):416-423.

[9] Jiang Z, Pflug K, Usama SM, Kuai D, Yan X, Sitcheran R, et al. Cyanine-Gemcitabine Conjugates as Targeted Theranostic Agents for Glioblastoma Tumor Cells. J Med Chem. 2019;62(20):9236-9245.

[10] Ribatti D. The chick embryo chorioallantoic membrane (CAM). A multifaceted experimental model. Mechanisms of Development. 2016;141:70-77.

[11] Nowak-Sliwinska P, Segura T, Iruela-Arispe ML. The chicken chorioallantoic membrane model in biology, medicine and bioengineering. Angiogenesis. 2014;17(4):779-804.

[12] Ghaffari-Tabrizi-Wizsy N, Passegger CA, Nebel L, Krismer F, Herzer-Schneidhofer G, Schwach G, et al. The avian chorioallantoic membrane as an alternative tool to study medullary thyroid cancer. Endocr Connect. 2019;8(5):462-467.

[13] Ribatti D. The Chick Embryo Chorioallantoic Membrane in the Study of Angiogenesis and Metastasis: The CAM assay in the study of angiogenesis and metastasis. Netherlands: Springer Dordrecht Heidelberg London New York; 2010. p. 45-63.

[14] Chen ST, Proctor CM, Malliaras GG. Materials and Device Considerations in Electrophoretic Drug Delivery Devices. Sci Rep. 2020;10(1):7185.

[15] Uguz I, Proctor CM, Curto VF, Pappa AM, Donahue MJ, Ferro M, et al. A Microfluidic Ion Pump for In Vivo Drug Delivery. Adv Mater. 2017;29(27).

[16] Seitanidou M, Tybrandt K, Berggren M, Simon DT. Overcoming transport limitations in miniaturized electrophoretic delivery devices. Lab on a Chip. 2019;19(8):1427-1435.

[17] Arbring Sjöström T, Berggren M, Gabrielsson EO, Janson P, Poxson DJ, Seitanidou M, et al. A Decade of Iontronic Delivery Devices. Advanced Materials Technologies. 2018;3(5):1700360.

[18] Poxson DJ, Gabrielsson EO, Bonisoli A, Linderhed U, Abrahamsson T, Matthiesen I, et al. Capillary-Fiber Based Electrophoretic Delivery Device. ACS Appl Mater Interfaces. 2019;11(15):14200-14207.

[19] Bernacka-Wojcik I, Huerta M, Tybrandt K, Karady M, Mulla MY, Poxson DJ, et al. Implantable Organic Electronic Ion Pump Enables ABA Hormone Delivery for Control of Stomata in an Intact Tobacco Plant. Small. 2019;15(43):e1902189.

[20] Belot N, Rorive S, Doyen I, Lefranc F, Bruyneel E, Dedecker R, et al. Molecular characterization of cell substratum attachments in human glial tumors relates to prognostic features. Glia. 2001;36(3):375-390.

[21] Xie Y, Bergström T, Jiang Y, Johansson P, Marinescu VD, Lindberg N, et al. The Human Glioblastoma Cell Culture Resource: Validated Cell Models Representing All Molecular Subtypes. EBioMedicine. 2015;2(10):1351-1363.

[22] Giakoumettis D, Kritis A, Foroglou N. C6 cell line: the gold standard in glioma research. Hippokratia. 2018;22(3):105-112.

[23] Yang C, Zhang J, Ding M, Xu K, Li L, Mao L, et al. Ki67 targeted strategies for cancer therapy. Clin Transl Oncol. 2018;20(5):570-575.

[24] Li LT, Jiang G, Chen Q, Zheng JN. Ki67 is a promising molecular target in the diagnosis of cancer (review). Mol Med Rep. 2015;11(3):1566-1572.

[25] Chen X, Zhang M, Gan H, Wang H, Lee JH, Fang D, et al. A novel enhancer regulates MGMT expression and promotes temozolomide resistance in glioblastoma. Nat Commun. 2018;9(1):2949.

[26] Kinra P, Malik A. Ki 67: Are we counting it right? Indian Journal of Pathology and Microbiology. 2020;63:98.

[27] Wittekind D. Traditional staining for routine diagnostic pathology including the role of tannic acid. 1. Value and limitations of the hematoxylin-eosin stain. Biotechnic & Histochemistry. 2003;78(5):261-270.